Study of water stress in riparian stands along a hydroclimatic gradient using thermal imagery and ecophysiological measirements

Auteur : Malherbe, Pauline
Promoteur(s) : Lejeune, Philippe; 22587
Faculté : Gembloux Agro-Bio Tech (GxABT)
Diplôme : Master en bioingénieur : gestion des forêts et des espaces naturels, à finalité spécialisée
Année académique : 2023-2024
URI/URL : http://hdl.handle.net/2268.2/19437

LIÈGE université
Gembloux
Agro-Bio Tech

STUDY OF WATER STRESS IN RIPARIAN STANDS ALONG A HYDROCLIMATIC GRADIENT USING THERMAL IMAGERY AND ECOPHYSIOLOGICAL MEASUREMENTS

PAULINE MALHERBE

TRAVAIL DE FIN D'ETUDES PRESENTE EN VUE DE L'OBTENTION DU DIPLOME DE MASTER BIOINGENIEUR EN GESTION DES FORÊTS ET DES ESPACES NATURELS

ANNEE ACADEMIQUE 2023-2024

CO-PROMOTEURS : PHILIPPE LEJEUNE & BAPTISTE MARTEAU

[1] L'autorité académique est représentée par les promoteurs membre du personnel enseignant de GxABT.

[2] The academic authority is represented by the thesis supervisor, a member of the GxABT teaching staff

LIÈGE université
Gembloux
Agro-Bio Tech

STUDY OF WATER STRESS IN RIPARIAN STANDS ALONG A HYDROCLIMATIC GRADIENT USING THERMAL IMAGERY AND ECOPHYSIOLOGICAL MEASUREMENTS

PAULINE MALHERBE

TRAVAIL DE FIN D'ETUDES PRESENTE EN VUE DE L'OBTENTION DU DIPLOME DE MASTER BIOINGENIEUR EN GESTION DES FORÊTS ET DES ESPACES NATURELS

ANNEE ACADEMIQUE 2023-2024

CO-PROMOTEURS : PHILIPPE LEJEUNE & BAPTISTE MARTEAU

Remerciements

La réalisation de ce mémoire a été encadrée par les laboratoires UMR 5600 EVS et 5023 LEHNA et le CNRS.
Le projet de recherche a été financé par l'OHM vallée du Rhône et FR BioEnviS.
La mobilité a été subventionné par la bourse Erasmus +.
La récolte de donnée en forêt a été effectuée par Lucas Andre, Julien Godfroy, Flavie Gerle, David Lafleuriel, Pierre Lochin, Pauline Malherbe, Baptiste Marteau et Antoine Vernay.
La récolte de données aéroportées ainsi que la formation aux logiciels de traitement été effectuée par Baptiste Marteau.
Le traitement des échantillons végétaux a été effectué par Antoine Vernay.
Merci au Conservatoire des Espaces Naturels Isère pour leur aide dans l'identification des sites et leur accompagnement dans l'obtention d'autorisations d'accès à la réserve naturelle.

Je tiens à remercier mes deux promoteurs pour leur accompagnement dans la réalisation de ce TFE depuis mon stage, leur relectures et leurs conseils avisés. Merci à Philippe Lejeune pour son encadrement, sa disponibilité et ses précieuses recommandations. Merci à Baptiste Marteau pour sa confiance, la formation à la recherche, sa bienveillance et l'intégration dans son projet de recherche.

De plus, je remercie Pierre pour ses speech de motivation, les inspirations, la confiance accordée et toute la collaboration pour mener à bien ce projet et Antoine pour ses relectures et ses précieux conseils pour l'analyse des résultats. Merci à tous les biogéophiles pour l'accueil à Lyon, la merveilleuse année passée au labo et le soutient.

Abstract

In the context of climate change and anthropogenic modifications, natural ecosystems must adapt to their environment at an unprecedented pace. Riparian forests are particularly sensitive to these alterations as they heavily rely on soil water availability for survival. Understanding the response of riparian trees to drought episodes is a significant asset for the management of forests and natural spaces.

In this study, a combined approach of remote sensing and ecophysiology was adopted to understand the response of white poplar trees to water constraints during a vegetative season and at a drought period along a hydroclimatic gradient. The objective was to identify responses and mechanisms adopted to face water stress at different spatial and temporal scales, as well as to assess their vulnerability to climate change.

The results obtained reveal a contrast in the mechanisms of drought response depending on the location of the stands along the hydroclimatic gradient. In the northern regions, there is a relative stability of NDVI during the season and a low relative temperature during the drought, but with very low values of water potential and leaf water content, indicating high water consumption. In contrast, further south, the opposite phenomenon was observed, with a rapid decrease in NDVI, higher temperature but higher ecophysiological indicators that respond more gradually.

Key words: Alluvial forest, Thermal infrared, Water stress, Populus Alba, Remote sensing, Hydroclimatic gradient

Résumé

Dans un contexte de changement climatiques et de modifications anthropiques, les écosystèmes naturels doivent s'adapter à leur environnement à un rythme sans précédent. Les forets alluviales sont des milieux particulièrement sensibles à ces altérations car elles dépendent fortement de la disponibilité en eau dans les sols pour survivre. Mieux comprendre la réaction des arbres ripariens face aux épisodes de sécheresse est un atout considérable pour la gestion des forêts et des espaces naturels.

Dans cette étude, une approche combinée de la télédétection et de l'écophysiologie a été adoptée afin de de cerner la réaction des peupliers blancs aux contraintes hydriques au cours d'une saison végétative et en moment de sécheresse le long d'un gradient hydroclimatique. L'objectif étant d'identifier les réponses et les mécanismes mis en place face au stress hydrique à différentes échelles spatiales et temporelles, ainsi que de pouvoir évaluer leur vulnérabilité face au changement climatique

Les résultats obtenus montrent un contraste entre les mécanismes de réponse à la sécheresse mis en place en fonction de la position des peuplements le long du gradient hydroclimatique. Au nord, ils montrent une relative stabilité du NDVI au cours de la saison et une température relative faible durant la sécheresse mais des taux de teneur en eau et de potentiel hydrique très faible, indiquant une forte consommation d'eau. Au contraire, plus au sud, le phénomène inverse a été observé, avec une baisse rapide du NDVI, une température élevée mais des indicateurs écophysiologiques plus hauts et qui répondent plus progressivement.

Mots clés : Foret alluvial, Infrarouge thermique, Stress hydrique, Populus Alba, Télédétection, Gradient hydroclimatique

Table of contents

1. Introduction

1.1. Research context

The increasing frequency and severity of droughts associated with global warming is threatening forest ecosystems (Choat et al., 2018; Peters et al., 2021; Reichstein et al., 2013). Large-scale forest mortality has been documented worldwide (Allen et al., 2010, 2015) and linked to drought and global warming (Anderegg et al., 2013; Choat et al., 2012; Greenwood et al., 2017; Hartmann et al., 2018). Among these ecosystems, riparian forests are particularly vulnerable to drought despite their location in lowland floodplains (Kibler et al., 2021; Williams et al., 2022). Soil moisture and groundwater availability are the primary requirements for long-term survival of most riparian tree species under drought conditions (Pettit & Froend, 2018). However, the increasing duration of droughts is reducing soil moisture (Samaniego et al., 2018) and streamflow (De Girolamo et al., 2022), weakening the functioning of these riparian tree species. In this context, developing a better characterization of water stress mechanisms in riparian forests is fundamental for assessing the risk of tree mortality, not only at the individual scale.

Because of their location in lowlands, riparian forests are naturally exposed and highly sensitive to fluctuations in water availability (Friedman et al., 2022; Shafroth et al., 2002). In response, most riparian tree species have developed several physiological and morphological adaptations to cope with water deficits, such as rapid root extension and low shoot:root biomass ratios (Rood et al., 2003; Stella & Battles, 2010). However, prolonged periods of water scarcity and anthropogenic alterations of streamflow and groundwater levels can severely reduce water availability inevitably affecting riparian tree growth and health. Drought-related growth decline and mortality have been documented in riparian trees, mostly in semi-arid environments (Pettit & Froend, 2018; Rivaes et al., 2013; Stromberg et al., 1996). More recently, studies have expanded the scope of interest by analyzing riparian forest responses to drought at the landscape scale (Kibler et al., 2021; Pace et al., 2021; Rohde et al., 2021). However, these studies only examined riparian stand responses without accounting for specific individuals nor for climate variability. As a result, our understanding of how riparian forests respond to evolving drought conditions remains limited (Portela et al., 2023; Slette et al., 2019), especially across hydroclimatic gradients (Palmer et al., 2008). By investigating the responses of specific riparian tree species to drought in diverse climates, the overall drought response strategies and resilience of riparian forests can better be understood.

1.2. Water stress

Increasing temperatures and reduced precipitation, which are characteristics of climatic drought, directly affect soil water availability (Berg & Sheffield, 2018). As temperatures rise, evaporative demand increases, leading to an increase in evapotranspiration, which directly controls water fluxes between soil, trees, and the atmosphere (Katul et al., 2012). As a result, reduced water availability alters soil-root and leaf-atmosphere interfaces, leading to limited water and CO_2 fluxes (Reichstein et al., 2002), severely limiting carbon assimilation and tree growth, and threatening tree survival. Water stress in plants is a complex physiological response to the limited availability of water (Teskey & Hinckley, 1986). These responses can induce a series of harmful plant-water interactions susceptible to disrupt plant's physiology. Under high evaporative demand and low soil water availability, water potential decreases, causing most species to close their stomata (Pirasteh-Anosheh et al., 2016). Prolonged periods of stomatal closure can lead to irreversible disruption of water transfer in xylem tissue due to the breakdown of water cohesion and massive vascular embolism (Bréda et al., 2006; Martinez-Vilalta et al., 2019). Deterioration of hydraulic function is the primary cause of drought-induced tree mortality (McDowell, 2011). Reduced growth and tree mortality can also be explained by carbon starvation, although this is less common than that caused by hydraulic failure (Hentschel et al., 2016; McDowell et al., 2008). Carbon starvation occurs when photosynthetic carbon assimilation is insufficient to meet the demands of cell maintenance and defensive metabolism (McDowell, 2011).

Trees adopt various strategies and behaviors to withstand episodes of water stress. These adaptations are either morphological, physiological, or biochemical and are designed to maximize productivity while limiting water loss (Lisar et al., 2012). Tree responses fall into two categories: those that resist stress and those that avoid stress. Some trees adopt relatively isohydric behavior, reducing stomatal conductance to limit water loss and maintain leaf water potential (Ψ_m), thereby exposing themselves to carbon starvation (Hentschel et al., 2016; Sevanto et al., 2014). Other trees adopt anisohydric behavior, keeping their stomata open to maintain high levels of transpiration and ensure carbon assimilation and growth, but at a higher risk of hydraulic failure (Sevanto et al., 2014). These ecophysiological responses are also accompanied by morphological changes such as leaf area reduction, canopy dieback, branch abscission, and reduced diameter growth (Stella & Battles, 2010). These different drought resistance mechanisms can vary within the same species and even more so at broad landscape scales. Various remote and ground-based technologies have been developed to measure tree water status.

1.2.1. Ecophysiological measurements

The most widely used and closely related proxy to water stress is water potential, which measures the potential energy of water in plant tissues and which is closely related to water stress. Relative water content (RWC) is another proxy that has gained popularity due to its ease of measurement and ability to serve as a good indicator of landscape-scale mortality (Martinez-Vilalta et al., 2019). However, these proxies cannot account for variations in CO_2 flux, upon which carbon assimilation depends. To address this limitation, the intrinsic water use efficiency index (WUE_i), an integrative measure of the balance between carbon and water fluxes, can be used to provide valuable information on carbon assimilation (Seibt et al., 2008). However, obtaining data through these ecophysiological measurements requires significant financial and time investments, particularly when working on large spatial and temporal scales.

1.2.2. Remote sensing measurements

To address these challenges, remote sensing tools have been developed to estimate vegetation water status and identify areas most affected by drought (Le et al., 2023). Remote sensing technologies can be cost-effective, display spatial patterns at a variety of scales, and reveal a variety of structural and physiological characteristics of water-stressed plants. Remote sensing tools use a range of spectral wavelengths to detect changes in the reflectance or thermal properties of plants. These technologies acquire many hundreds of spectral bands across the spectrum from 400 nm to 2 500 nm, using satellite, airborne or hand-held devices (Govender, 2009). Plant water content at the leaf and canopy scales can be estimated using specific spectral reflectance bands and indices from near infrared, middle infrared and short-wave infrared regions of the electromagnetic spectrum (Tucker, 1980; Hunt and Rock, 1989; Gao, 1995; Zarco-Tejada et al., 2003; Jackson et al., 2004; Shen et al., 2005; Chun-Jiang et al., 2006 in Govender, 2009). Many parameters play a role in the spectral reflectance of a plant, such as species, site, age or maturity of plants or foliage, nutrient status, and leaf orientation, effects of variable irradiance, variable background, and the geometrical arrangement of the object/scene, sensor, and surface, orientation of the ground surface in relation to the location of the sun and remote sensing device and meteorological conditions (Asner, 1998).

Vegetation indices based on reflectance in the visible or near-infrared, such as NDVI and NDWI, are primarily used to estimate leaf chlorophyll or leaf water content (Le et al., 2023). Several studies have shown significant relationships between changes in greenness and water availability (Aguilar et al., 2012) permitting to relate on the evolution of NDVI through seasons to deduct the water availability

of vegetation (Lochin et al., *in prep*.). In addition, thermal radiation emitted by trees is widely used to estimate tree water status, as canopy temperature is a reliable proxy for transpiration (Fuchs, 1990). When plants experience water stress, they close their stomata to reduce water loss, which in turn reduces evaporative cooling. This causes the temperature of the plant canopy to equilibrate with ambient conditions. In contrast, well-hydrated plants can maintain transpiration and evaporative cooling, resulting in cooler canopy temperatures (Surendar, 2013). Therefore, canopy temperature can be used as a direct indication of plant water stress.

1.3. Objectives and approaches

The combined use of ecophysiological indicators and remote sensing is commonplace in agronomy to assess water stress in crop plantations in environments heavily influenced by human activities (Ben-Gal et al., 2009; Berni et al., 2009). These studies have demonstrated significant correlations between remotely sensed water stress indicators and ecophysiological measurements. However, this combination of tools has rarely been used to study the water stress responses of trees or forests, particularly in natural ecosystems. Recent work has demonstrated the potential of these tools to assess forest water status and health at large scales (Marusig et al., 2020). But to our knowledge, few studies, if any, have combined these tools to assess water stress responses of riparian forests at the landscape scale, taking into account climatic variability.

This study aims to combine ecophysiological and remote sensing measurements to estimate the water status of white poplar (*Populus alba L.*) during the seasonal progression of drought at three sites, located within riparian forests and across a strong climatic gradient. In addition, two levels of remotely sensed data were used with differing yet complementary objectives, i.e., satellite and airborne imagery. These tools combined should be able to provide insights into the responses of riparian trees to drought along a climatic gradient, as well as into the water stress resistance mechanisms developed by this species. The role of local water availability in the resistance and resilience of Populus alba to drought was also assessed. Generally, the climatic gradient allows to hypothesize about the future resistance of forests in environments less accustomed to water stress. Two working hypotheses concerning southern regions, often characterized by Mediterranean climates, and so more prone to intensified and prolonged drought events, were used:

1) Trees in southern regions are more susceptible to the impacts of drought;
2) A warmer canopy coupled with a low NDVI indicates compromised ecophysiological health.

2. Methods

2.1. Regional context and study sites

The study area focuses on the French Rhône corridor, a major European river flowing between Geneva and the Mediterranean Sea. Its catchment area in France covers 90,500 km^2 with a mean annual discharge of 1,700 m^3/s at its mouth (Olivier et al., 2022). This river corridor is mainly north-south oriented (Fig. 1a) and is characterized by an important hydroclimatic gradient, from drier and warmer conditions in the south to wetter and cooler conditions in the north (Sargeant & Singer, 2021; Sauquet et al., 2019). This hydroclimatic gradient strongly influences the growth and health of riparian trees, which are sensitive to both local climatic context and non-local climate forcing (Lochin et al., 2023; Sargeant & Singer, 2021). Despite these climatic differences, riparian forests along this hydroclimatic gradient are homogeneous in terms of species and distribution (Olivier et al., 2022). They are primarily dominated by a combination of early successional trees, including *Populus nigra, Populus alba,* and *Salix alba,* and post-pioneer trees, such as *Fraxinus excelsior* and *Acer platanoides* (Räpple, 2018). These forests are also home to invasive species, such as *Acer negundo* and *Robinia pseudoacacia* (Janssen et al., 2020).

The Rhône is a highly anthropized river that has undergone several large-scale development projects since the 19th century. The most recent and impactful has been the construction of sixteen dams and diversion canals for hydropower generation (Lamouroux et al., 2015; Olivier et al., 2022). These structures have altered hydrological, sedimentary, and ecological flows, particularly in the Old Rhône, the former main channel, where flows have been reduced by 95% following the creation of diversion canals (Bravard & Gaydou, 2015; Vázquez-Tarrío et al., 2019). These hydrological consequences, combined with the incision of the Rhône and the lowering of water levels due to the high frequency of low minimum discharge, have led to a sudden drop in water levels and a significant disconnection of alluvial stands (Olivier et al., 2022).

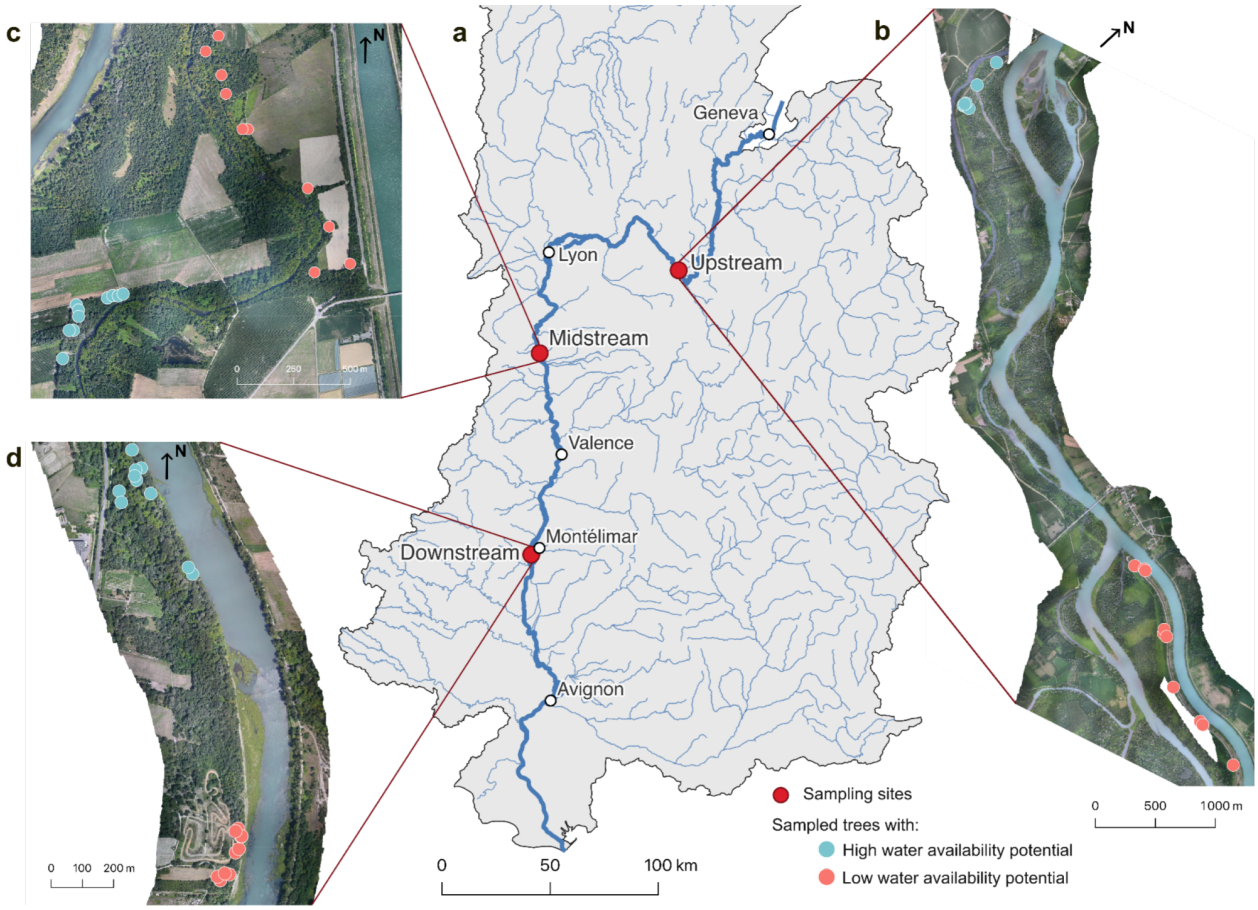

Fig. 1 (a) Location of the 3 study sites along the Rhône and of the 20 trees per site, classified according to the level of water availability (LWAP and HWAP) for (b) the upstream site, (c) the midstream site, and (d) the downstream site.

To account for hydroclimatic differences, three sites were selected (Fig. 1a) distributed along the Rhône River: Brégnier-Cordon (hereafter referred to as upstream, Fig. 1b), Péage-de-Roussillon (midstream, Fig. 1c), and Donzère-Mondragon (downstream, Fig. 1d). At these three sites, the climatic averages over the growing season from May to August between 1995 and 2023 showed a significant difference. The average air temperature at the upstream site was 19.1°C, with an average cumulative rainfall of 373 mm. At midstream, these values were 20.1°C and 244 mm, respectively, while at downstream they were 22.1°C and 183 mm, respectively (data from E-OBS). In addition, to represent equivalent hydrological conditions, the three sites are among some bypassed reaches, each characterized by two plots with clear differences in water availability conditions.

2.2. Plot selection and target species

The goal being to select plots with high or low water availability, the degree of connection of riparian stands to the water table was approximated. To this end, a proxy for water availability based on remote sensing information was used (explained in Section 2.3.2) and identified plots with potentially high and plots with potentially low groundwater availability at each site. This step, with the field survey, was the first one in the workflow of this study, as shown in Figure 2.

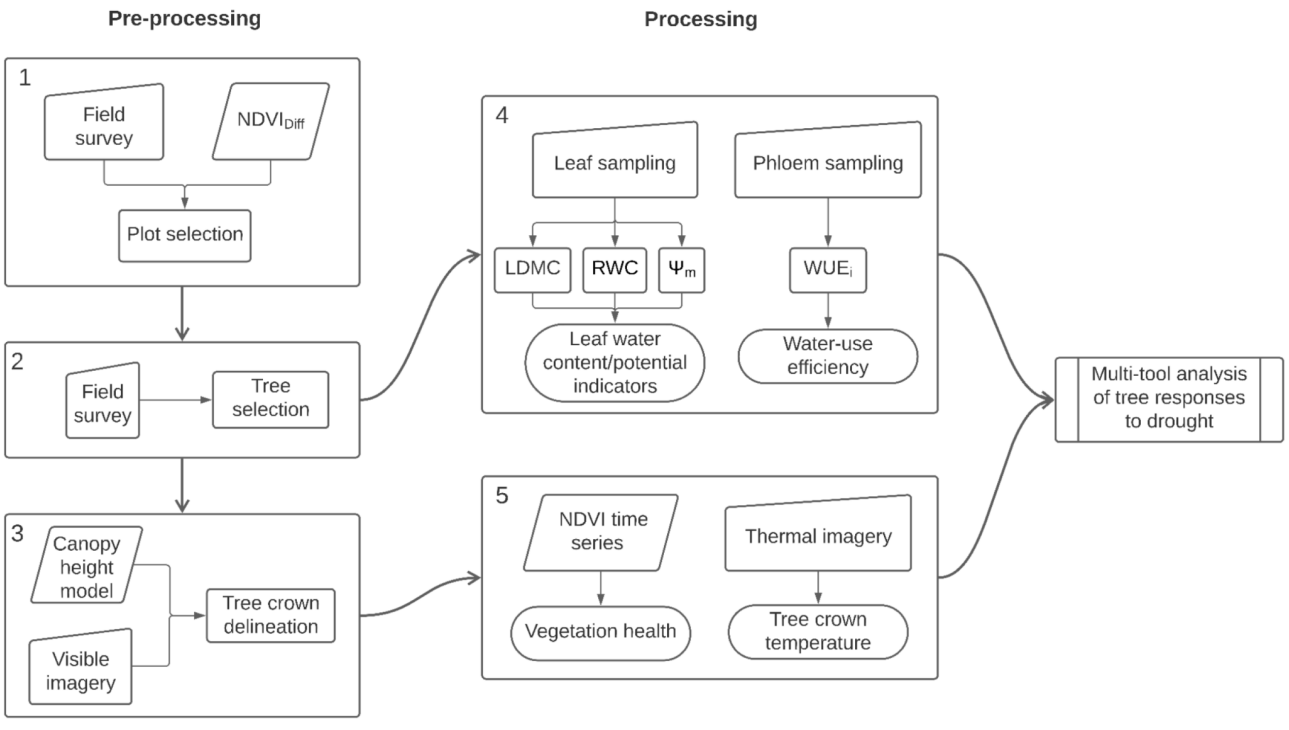

Fig. 2 - General workflow and study design of the methods for the pre-processing and the processing steps. The different shapes surrounding the steps help to identify the different types of data sources and results. Polygons with different heights represent data collected in the field during the season, parallelograms are external data, rectangles are intermediate results, while rounded-corner rectangles indicate the final data used for analysis.

Both local knowledge and an overview of previous studies along the Rhône corridor have pointed out members of the Salicaceae family as insightful and strategic model trees to study tree response to droughts. The studied species is the white poplar, renowned for its contributions to the rehabilitation of degraded land and restoration of forest landscapes (Isebrands & Richardson, 2014). White poplar is a phreatophyte species that relies heavily on root connections to the alluvial water table (Sánchez-Pérez et al., 2008; Sargeant & Singer, 2021; Singer et al., 2013). It is one of the dominant species in Rhône alluvial forests (Olivier et al., 2022). To conduct the study ten white poplars were selected from each of the high water availability potential (HWAP) and low water availability potential (LWAP) plots at each of the three sites. To our knowledge, no accurate forest inventory has been

conducted along the latitudinal gradient of the study area. Therefore, our objective was to capture the variability in tree size. Mature trees with a mean diameter of 62.6 cm (+/- 25.1 cm) and a mean height of 21.3 m (+/- 4.9 m) were carefully selected. The circumference was measured at breast height using a measuring tape and extracted tree heights from a canopy height model developed using data from the LiDAR HD program of the French National Geographic Institute (https://geoservices.ign.fr/lidarhd). Each tree was located using high-accuracy DGPS (Geomax Zenith 35 Pro). Trees were selected based on three criteria: (1) ease of access to enable regular sampling; (2) availability of low-hanging, reachable branches; and (3) visibility of the entire canopy from above to ensure clear identification of trees in aerial images.

2.3. Satellite remote sensing acquisition and processing

2.3.1. NDVI time series

Sentinel-2 satellite imagery was used to assess the vegetative responses of individual trees over time. These satellites provide imagery with a spatial resolution of 10-20 m and a temporal resolution of six days over our study area (Li & Roy, 2017). Images with less than 30% cloud cover were downloaded and processed with a cloud mask, using Google Earth Engine (Gorelick et al., 2017). They were used to calculate the Normalized Difference Vegetation Index (NDVI) to quantify the dynamics of riparian tree health during the growing season. NDVI was calculated using the following formula:

$$NDVI = \frac{NIR - R}{NIR + R} \quad (1)$$

where NIR corresponds to Sentinel-2 satellite band 8 and R corresponds to the visible red band (i.e., band 4). Median NDVI values were extracted from the canopy of each sampled tree. Canopy polygons were delineated using the method described in Section 2.4 (Fig. 4d). In total, the NDVI time series for the growing season of 2023 consists of 168 images covering the three sites.

2.3.2. $NDVI_{Diff}$ index

Median NDVI images were obtained for each site and plot in June and August 2022. We calculated $NDVI_{Diff}$ from these median images using the method developed by Lochin et al. (*in prep*.). The $NDVI_{Diff}$ index shows the evolution of NDVI between June and August, distinguishing areas where NDVI decreases from those where it remains stable. The $NDVI_{Diff}$ index was used as a proxy

for water availability. Lochin et al. (*in prep*.) showed how this index applied to the midstream site was related to water availability in the phreatic zone for white poplars. We used data from the summer 2022 to calculate $NDVI_{Diff}$ because it was, on average, the second hottest summer in France since 1900 and one of the driest on record (Guinaldo et al., 2023; Tripathy & Mishra, 2023). Using $NDVI_{Diff}$ over the 2022 growing season, we were able to differentiate plots with potentially high phreatic water availability from those with potentially low water availability (Fig. 3).

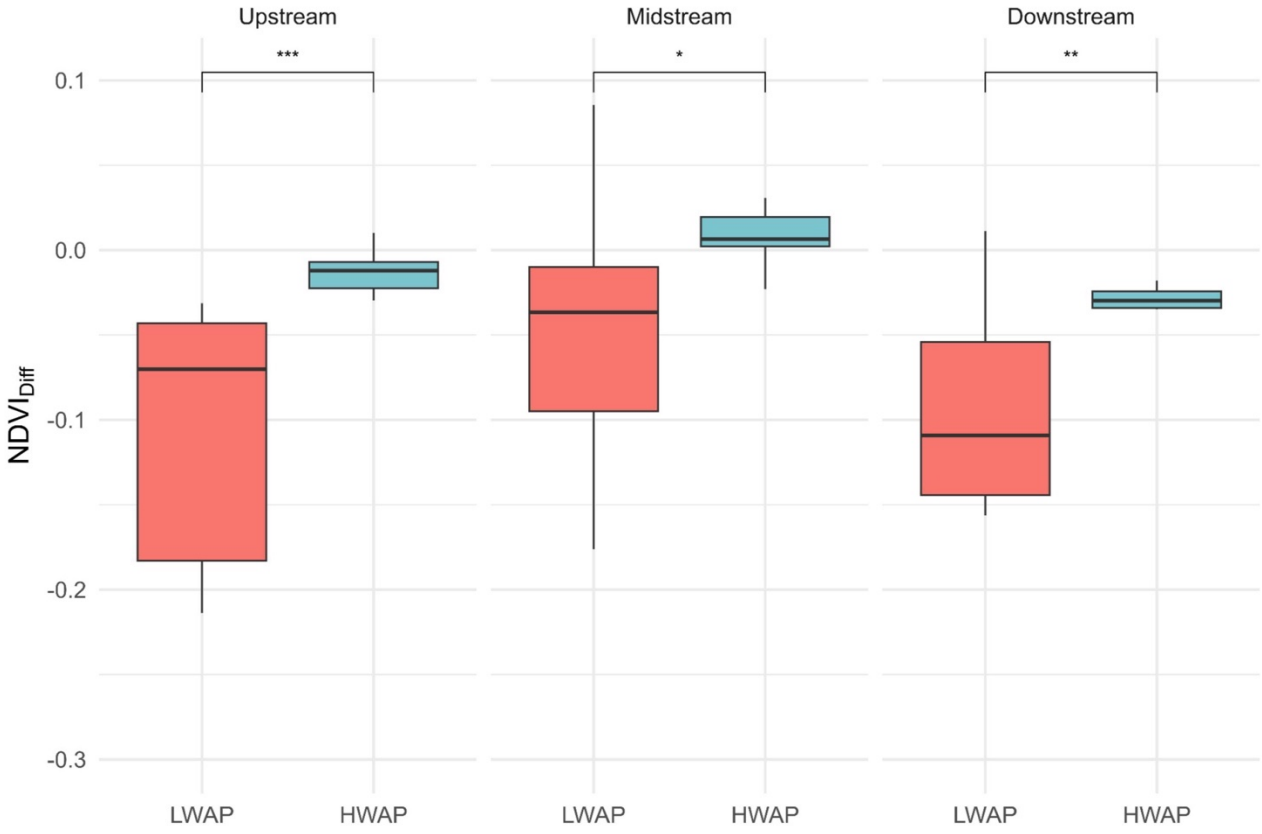

Fig. 3 - Comparison of $NDVI_{Diff}$ values on each plot (LWAP and HWAP) and on each of the three sites (upstream, midstream, downstream). * indicates that the difference between means is statistically significant according to the Wilcoxon test, with *** indicating $p < 0.001$, ** = $p < 0.01$, * = $p < 0.05$, and ns = $p > 0.05$.

2.4. Airborne remote sensing acquisition and processing

2.4.1. Aerial data collection

Aerial imagery was collected using an ultralight trike. Two cameras were carried during the flight to collect data in the visible (RGB) and thermal infrared (TIR) domains. The cameras were mounted on a stabilizer to provide clear images despite the motion induced during the flight. Each camera was programmed in time-lapse mode to take an image every 2 seconds and was connected to an external battery and a laptop to adjust the focus during the flight, if necessary. The visible camera

was a Nikon Z 6 II (30 mm lens) with a resolution of 6048 × 4024 pixels and was connected to a GPS transmitter. The thermal infrared camera was a VarioCam HD head with a resolution of 1024 x 768 pixels, which senses infrared radiation in the 7.5 - 14 µm range. Each site was overflown between 11:30 a.m. and 12:30 p.m. on days with clear skies and no precipitation over the previous 24 h. Average flight altitude was 500 m, resulting in visible images with a resolution of 6 cm·pixel^{-1} and 30 cm·pixel^{-1} for the TIR images. Campaigns were conducted on 12 (downstream), 17 (upstream), and 18 (midstream) July 2023, concurrent with tree sampling.

2.4.2. Aerial data processing

Each set of images was processed separately using the Agisoft Metashape Professional 2.0.2 software. First, RGB images were imported into the software in their original format (.jpeg) and georeferenced. Then, in QGIS (3.32), the alignment was optimized using markers based on the latest IGN Ortho 20 cm orthophotos and IGN high-resolution LiDAR. The generated orthophoto had a resolution of 6 cm. The infrared thermal images, originally in .raw format, were then post-processed into .tiff using Irbis Pro 3.0 (InfraTec Gmbh©). To generate the final thermal orthomosaic, thermal images were first aligned using existing GPS information and then carefully aligned on the previously generated orthophoto. The exported thermal orthomosaics were composed of a single band (temperature in Kelvin), converted to °C, with a resolution of 30 cm·pixel^{-1}.

2.4.3. Canopy delineation and values extraction

Considering that it is preferable to measure canopy temperature by averaging all the leaves (Jones et al., 2009), the mean value of the entire canopy was extracted for each tree. To do this, each sampled tree was identified using high-precision DGPS (Geomax Zenith 35 Pro). Canopies were delineated using high-resolution orthophotos (Fig. 4a), and a digital height model derived from high-definition Lidar data obtained from IGN (Fig. 4b). Extraction from these polygons resulted in 60 values (i.e., 20 per site) of mean canopy temperature (T_c) (Fig. 4c). We then calculated the canopy temperature relative to air temperature (T_a) at the time of the survey (ΔT_{c-a}). This standardization allowed us to overcome the climatic differences between sites and flights, and is a reliable estimator of tree water use (Gonzalez-Dugo et al., 2012; Hernández-Clemente et al., 2019; Lapidot et al., 2019).

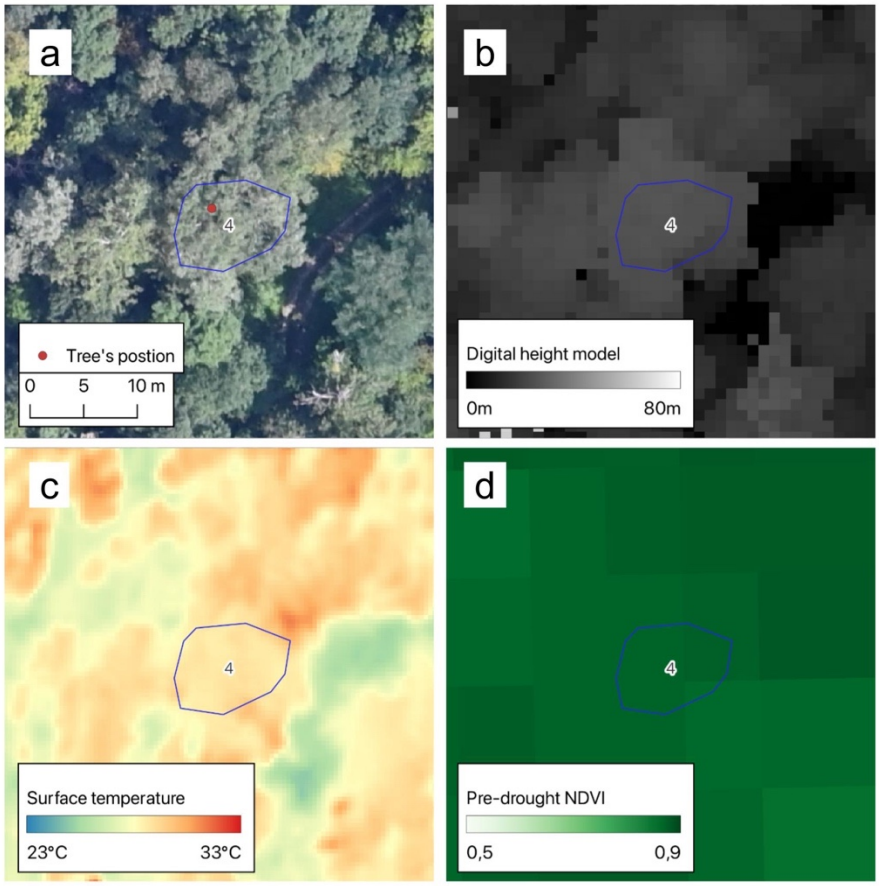

Fig. 4 (a) High resolution ortophoto of the forest area and (b) digital height model to visualize the canopy in order to extract (c) the surface temperature and (d) the NDVI. Example of canopy delineation for the tree 4 at Midstream.

2.5. Leaf trait measurements

2.5.1. Minimum leaf water potential

During the growing season, we measured the minimum leaf water potential (Ψ_m, MPa) every three weeks at all sites and plots (see Fig. 5). We collected a branch with leaves from each tree between 11:00 a.m. and 2:00 p.m. We then selected two green leaves and placed them in an aluminum bag with wet paper inside to maintain high humidity levels under dark conditions. Finally, we stored the branches in a cooler box until measurements, approximately 3 hours later. A preliminary experiment showed that Ψ_m did not vary significantly whether measured immediately after sampling or 3 hours later (data not shown). Back in the laboratory, Ψ_m was determined for each selected leaf using a pressure chamber (mod. 1505D, PMS Instrument Company, Albany, OR, USA 1505D, Scholander et al. 1965). The mean of the two measured leaves per tree was then used as a single replicate. Some trees were inaccessible due to broken branches or dieback during the season. The number of samples obtained at each site for each sampling is condensed in Section 8.1. (see S.I.).

2.5.2. Leaf dry matter content

On each sampling date, ten additional green leaves were also collected from each tree and weighed in the laboratory in three stages: (1) fresh weight (FW, g) measured directly after sampling, (2) turgid weight (TW, g) measured after being immersed in water for 12 hours, and (3) dry weight (DW, mg) following 48h of drying in an oven at 80°C. Using the FW and DW, we calculated the leaf dry matter content (LDMC), as follows (Pérez-Harguindeguy et al., 2016):

$$LDMC = \frac{FW}{DW} \quad (2)$$

2.5.3. Relative water content

Metrics measured as reported above also allowed the calculation of the relative water content (RWC, %) according to the formula developed by Smart and Bingham (1974):

$$RWC = \frac{FW - DW}{TW - DW} \quad (3)$$

2.6. Phloem sampling and $\delta^{13}C$ measurements

Phloem of all trees was sampled on each plot and each of the three sites, concomitantly with leaf sampling. Phloem discs were collected at breast height using a 9-mm diameter cork-borer. Such sampling, even when repeated during the experiment, does not critically affect tree function (Portier et al., 2023). Bark and wood were carefully removed to isolate the active phloem, which was then immersed in a 2.5 mL vial containing 1.5 mL of exudation solution (15 mM polyphosphate buffer: sodium hexametaphosphate, Sigma, München, Germany). Exudation lasted for five hours (Gessler et al., 2004) before the phloem disc was removed. The exudate solution was then stored in a freezer until all samples were ready for freeze-drying. The solutes were redissolved in 150 µL de-ionised water and the resulting solution was pipetted into tin capsules and dried at 60°C for 12 hours. Samples were then loaded into an elemental analyzer coupled to an isotope ratio mass spectrometer for $\delta^{13}C$ analysis performed at the LEHNA isotopic platform. Isotopic results were expressed in ‰ relative to VPDB (Vienna Pee Dee Belemnite).

To estimate the isotopic discrimination against ^{13}C ($\Delta^{13}C$, ‰), we combined atmospheric and phloem $\delta^{13}C$ values. $\delta^{13}C_a$ at middle latitudes can be considered constant at -8‰ (Yakir & Sternberg, 2000). Δ was then calculated as follows:

$$\Delta = \frac{\delta^{13}C_a - \delta^{13}C_p}{1+(\frac{\delta^{13}C_p}{1000})} \quad (4)$$

There are ongoing debates among specialists as to whether $\delta^{13}C_p$ correctly represents fresh photosynthates (e.g., Offermann et al., 2011). We acknowledge that post-photosynthetic pathways might alter the $\delta^{13}C_p$, but our previous work suggests that these effects are negligible (Vernay et al., 2020).

Intrinsic water use efficiency (WUE_i, µmol CO_2 mol H_2O^{-1}) was determined for each tree according to Seibt et al. (2008) for each sampling date:

$$WUE_i = \frac{C_a}{r} \times \left[\frac{b - \Delta - f \times \left(\frac{\Gamma*}{C_a}\right)}{b - a_a + (b - a_i) \times \frac{g_s}{g_m}} \right] \quad (5)$$

where C_a is atmospheric CO_2 concentration (µmol mol^{-1}), r the ratio of diffusivities of water vapor relative to CO_2 in the air (1.6), b the fractionation ratio during carboxylation (29‰), *f* the fractionation ratio during photorespiration (16.2‰, Evans and Von Caemmerer 2013), a_a and a_i the fractionation ratio of the diffusion through the air (4.4‰) and of diffusion and dissolution in water (1.8‰), respectively, and g_s/g_m the ratio of stomatal to mesophyll conductance. The CO_2 compensation point (Γ*, µmol mol^{-1}), was calculated according to the following formula (Medlyn et al., 2002):

$$\Gamma* = 42.75 \times e^{\frac{37830 \times (T_K - 298)}{298 \times T_K \times R}} \quad (6)$$

with T_K the ambient temperature (K) and *R* the universal gas constant (8.314 J mol^{-1} K^{-1}). g_s/g_m was considered constant, increasing the accuracy of WUE_i estimates (Vernay et al., 2020). Although we did not estimate this ratio in this experiment, we used a value of 0.51 determined on poplar species (Théroux-Rancourt et al., 2014). Previous work showed that daytime respiration would have a negligible effect on WUE_i, so this parameter was neglected to avoid introducing additional

uncertainty (Vernay et al., 2020). A more detailed description has been published recently, describing more accurately the different sampling steps in the field (Gerle et al., 2023).

2.7. Analysis of climate data and characterization of drought periods

To characterize meteorological conditions for 2023 at the three sites, we used the E-OBS gridded dataset (https://www.ecad.eu/), which provides daily weather data with a spatial resolution of 0.1 degrees (~11 km) (Cornes et al., 2018). Specifically, we extracted mean air temperature (TG), minimum air temperature (TN), maximum air temperature (TX), precipitation sum (RR), mean sea level pressure (PP), mean wind speed (FG), mean relative humidity (HU), and global radiation (QQ) at a daily time step between 1995 and 2023.

From these data, we calculated the daily reference evapotranspiration (ET_0) using the Penman-Monteith approach (Allen et al., 1998; Pohl et al., 2023). We used daily ET_0 to calculate the Standardized Precipitation Evapotranspiration Index (SPEI) (Beguería et al., 2010; Vicente-Serrano et al., 2010). SPEI is one of the most popular and accurate indices for characterizing drought conditions. It is derived from the original Standardized Precipitation Index (SPI), but differs in that it includes evapotranspiration. A negative SPEI indicates a relatively dry climate, while a positive SPEI indicates a relatively wet climate (Vicente-Serrano et al., 2010). To account for vegetative response lags, we calculated daily SPEI instead of the commonly used monthly time step. Daily SPEI allows us to overcome the temporal resolution of monthly SPEI and helps us to more accurately identify drought onset (Jia et al., 2018; Wang et al., 2021). It has also been shown to be as accurate as the monthly SPEI (Zhang et al., 2023), especially when estimated from the E-OBS dataset (Pohl et al., 2023). We computed a 30-day rolling SPEI value because it is the most commonly used timescale for identifying meteorological drought (Wang et al., 2014). The 30-day SPEI was used to estimate drought conditions in 2023 at each site and identify different periods of drought within the growing season (Fig. 5).

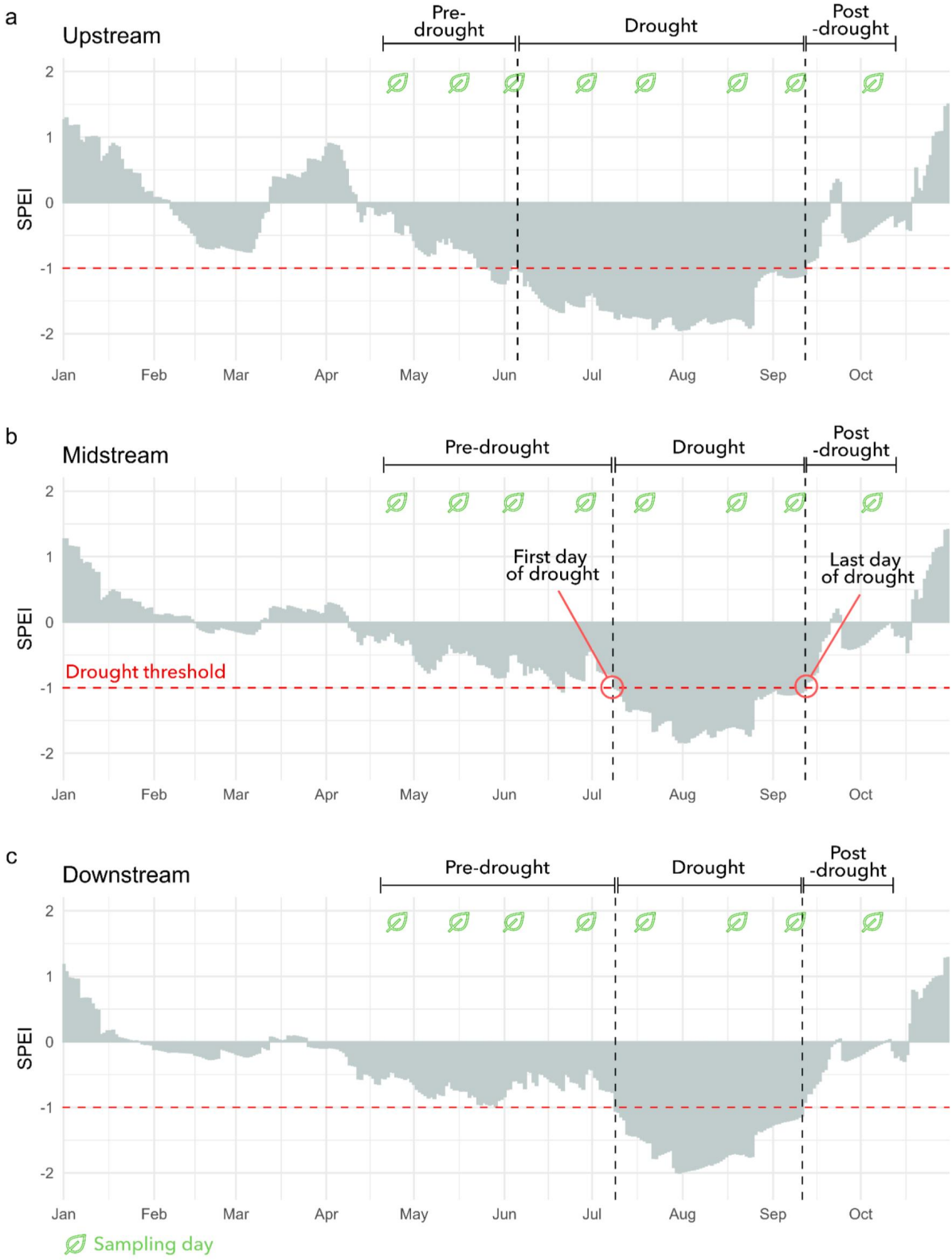

Fig. 5 - Evolution of the 30-day SPEI from January 1 to October 31 at the three sites. The two black dotted lines represent the start and end dates of the drought at each site, while the red dotted line represents the drought SPEI threshold. Green leaves indicate the days on which samplings were conducted.

Threshold analysis was performed to identify the different periods of drought within the growing season. We used a threshold of SPEI < -1 to define a state of drought, as it is commonly employed in

several studies (B. Ma et al., 2020; Q. Ma et al., 2023; Wang et al., 2014). The growing season was divided into three distinct phases: (1) the pre-drought phase (hereafter referred to as Pre- in figures), which extended from the first sampling date to the point when the SPEI continuously below -1 for at least 30 consecutive days; (2) the drought phase, characterized by SPEI values below -1; and (3) the post-drought phase (hereafter referred to as Post- in figures), which began when the SPEI exceeded -1 and continued until the last sampling date. At the three sites, the starting dates of drought differed (see S.I. Fig. S2), indicating an earlier onset of drought in the upstream section (158 DOY, June 7) than in the midstream (190 DOY, July 9) or downstream sections (190 DOY, July 9). The pre-drought phase began with our first sampling date and the post-drought phase ended with our last sampling date (see S.I. 8.1.).

2.8. Statistical analysis

In this study, three sites were sampled, each with 20 trees of different diameter. This variability in tree diameter may affect the ecophysiological responses of the trees. To assess the variance of WUE_i and Ψ_m and to determine whether there was a significant plot effect, multiway ANOVA was performed for each variable as a function of tree diameter and analyzed whether the diameter effect was significant. Wilcox test was used for pairwise comparison of the mean NDVI across drought periods (pre-drought, drought, and post-drought) and water availability plots (LWAP and HWAP). The same method was used to compare the means of each sampling date between each plot (LWAP and HWAP) for WUE_i and Ψ_m. Finally, the variances of WUE_i, Ψ_m, RWC, and LDMC was analyzed at each site and for each drought period and performed post-hoc pairwise comparisons using Tukey's estimated marginal means with the 'emmeans' R package (Lenth, 2023). All data analyses and statistical tests were performed using the R programming language (R Core Team, 2022, version 4.3.0).

3. Results

3.1. Multi-temporal NDVI analysis

NDVI analysis revealed distinct seasonal patterns at the three study sites along the hydroclimatic gradient (Fig. 6). The downstream site showed a significant decrease (p = 0.01) in NDVI values between pre-drought and drought, and then a slight but not significant increase until the post-drought period (p = 0.59). The dynamics of the mean NDVI were significantly affected by the

high variability between plots. Specifically, only the downstream site showed significant differences between HWAP and LWAP for each drought period ($p < 0.01$), with NDVI values significantly higher when water was potentially available (HWAP > LWAP). Differences in water availability conditions did not appear to affect NDVI at the up- and midstream sites, except during drought ($p = 0.001$) at the upstream site and during pre-drought at the midstream site ($p = 0.009$).

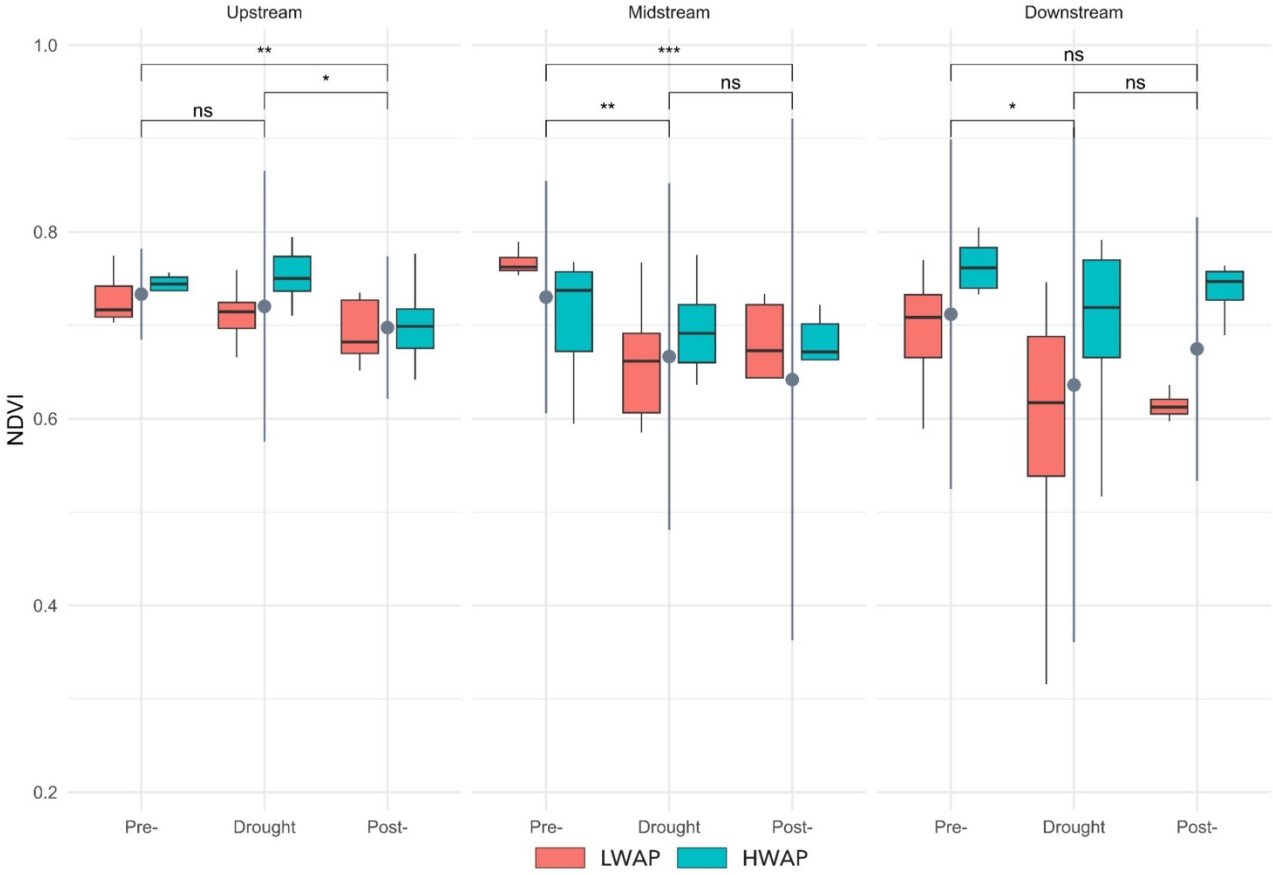

Fig. 6 - NDVI boxplots over the three drought phases (Pre-drought, Drought, Post-drought) between each plot (LWAP and HWAP) and each site (upstream, midstream, downstream). Gray dots show the mean NDVI per site and drought phase. * indicates that the difference between means is statistically significant according to the Wilcoxon test, where *** indicates $p < 0.001$, ** = $p < 0.01$, * = $p < 0.05$, and ns = $p > 0.05$.

At midstream, mean NDVI showed the same pattern as downstream, with a significant decrease between pre-drought and drought ($p = 0.004$), followed by relative stabilization after drought ($p = 0.87$). Upstream, the situation was reversed, with a relative stabilization between the first two phases ($p = 0.97$), followed by a significant decrease after drought ($p = 0.014$). Overall, during the growing season, NDVI decreased significantly between the pre-drought and post-drought periods at the upstream and midstream sites ($p = 0.009$ and $p < 0.001$, respectively) but not at downstream ($p = 0.074$), mainly because of the high variability between plots.

3.2. Multi-temporal ecophysiological analysis

To analyze the dynamics of WUE_i and Ψ_m and to help with their interpretation, we calculated mean values per plot and per site. We first tested whether there was any variability introduced by differences in diameters. The results showed two different responses: WUE_i showed no relationship with tree diameter (p = 0.739, F = 0.113), while it had a significant effect on Ψ_m (p = 0.001, F = 11.52). By including the interaction effect between tree diameter and site in the model, we observed no significant effect of diameter at each site on Ψ_m (p = 0.140, F = 2.04) and WUE_i (p = 0.830, F = 4.39). This suggests that variability in tree diameter at the site level did not have a significant effect on these two ecophysiological indicators, allowing us to average values by plot and site having to remove a potential diameter effect.

Analysis of the dynamics of the minimum leaf water potential (Ψ_m) during the growing season showed a similar overall trend among sites (Fig. 7a). Ψ_m decreased from the beginning of the growing season and reached a minimum in late August and early September, before increasing at a different pace depending on site and plot. This evolution of Ψ_m did not differ between plots with different water availability conditions, except upstream, where a significant difference between HWAP and LWAP was observed across four sampling dates (Fig. 7a). A similar seasonal pattern was observed for WUE_i at all three sites (Fig. 7b), with a slight increase at the beginning of the growing season until July, followed by a decrease to a minimum in late August and early September. Finally, WUE_i appeared to increase again at the last sampling date. This seasonal pattern was consistent for each site and plot, except downstream where the LWAP plot showed little variability during the growing season. Overall, differences in water availability conditions at each sampling date did not significantly affect the variability of Ψ_m (p = 0.298, F = 1.085) and WUE_i (p = 0.773, F = 0.084), so we further assessed their seasonal dynamics without considering plots.

The seasonal evolution of Ψ_m during the different phases of drought showed significant differences between sites (Fig. 7c). Pre-drought Ψ_m values were significantly different between sites, with a higher leaf water potential upstream than down- and midstream. After this initial phase, a significant decrease in Ψ_m occurred during the drought phase, but the magnitude of the change differed between sites. A minimum value (-3.38 MPa) was found upstream, which was significantly different from the other two sites. This inter-site difference was also observed in the post-drought phase, where downstream Ψ_m was significantly different from upstream and midstream, indicating that Ψ_m recovered to levels similar to pre-drought.

The seasonal pattern of WUE_i (Fig. 7d) was similar at up- and downstream sites, with a gradual decrease in WUE_i throughout the growing season, but was highly contrasted at midstream. The initial state (i.e., pre-drought) was similar at all three sites. Then, between pre-drought and post-drought, a significant decrease was observed at all sites, but more pronounced at midstream. After the drought, upstream and downstream WUE_i remained low. In contrast, midstream WUE_i returned to pre-drought levels. Although patterns and means were not significantly different between up- and downstream, variability was higher upstream than downstream, indicating that individual trees did not respond uniformly throughout the growing season.

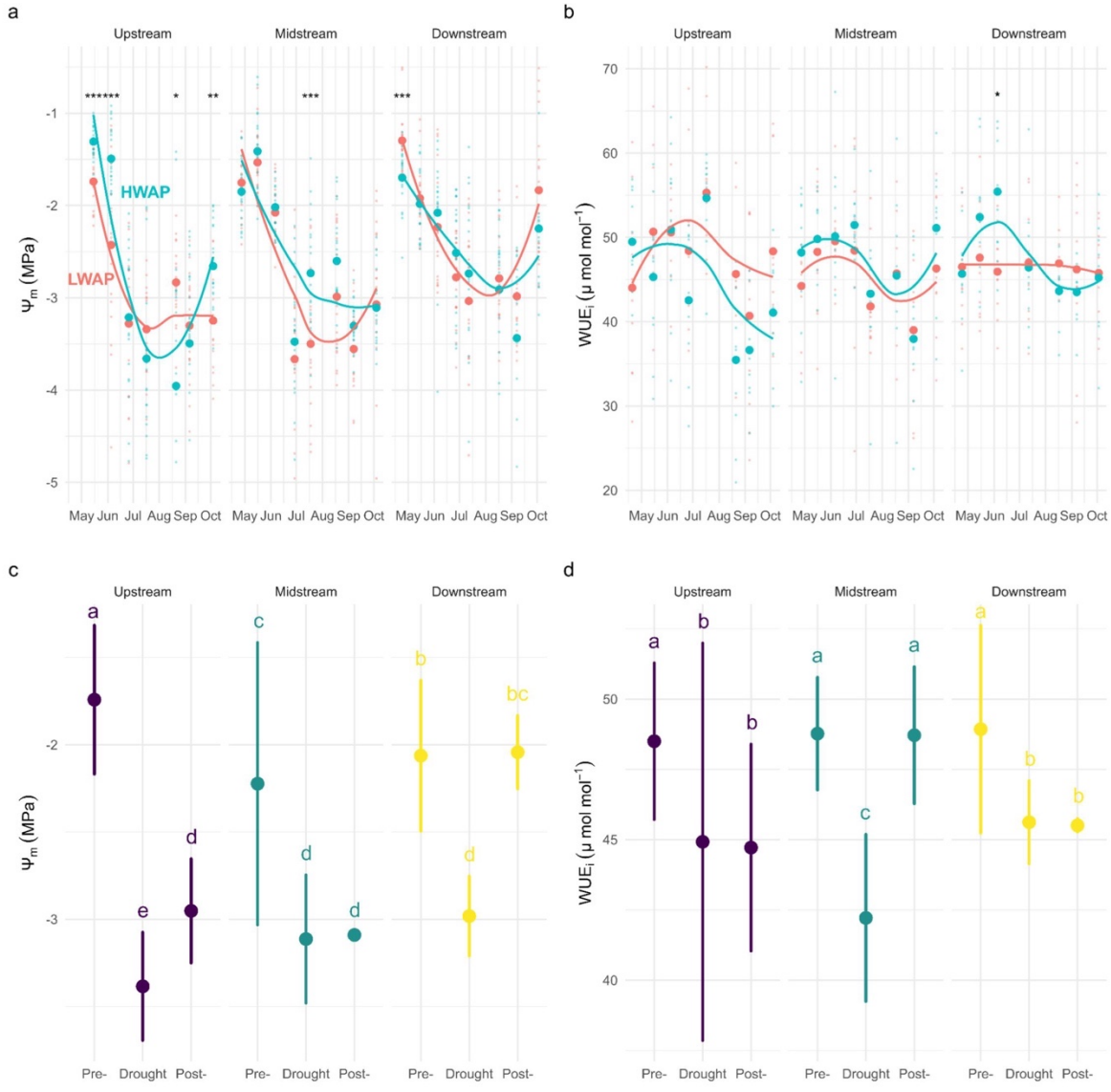

Fig. 7 - Dynamics of (a) minimum leaf water potential (Ψ_m) and (b) intrinsic water use efficiency (WUE_i) on each plot (LWAP, HWAP) and each sampling date. Mean values of (c) Ψ_m and (d) WUE_i over each drought phase among the three sites. Colors are for site identification only.* indicates that the difference between means was statistically significant according to the Wilcoxon test. Means without common letters were significantly different at the 95% confidence level ($p < 0.05$) in Tukey's HSD post hoc tests.

Figure 8 provided further evidence that white poplars did not behave similarly along the hydroclimatic gradient throughout the season. Leaf dry matter content (LDMC) was higher upstream ($p < 0.001$) throughout the growing season (Fig. 8a), indicating a higher proportion of dry matter in the leaves of trees upstream. Similarly, the seasonal pattern of LDMC showed significant differences in mean values between upstream and downstream sites in each phase (except for pre-drought) (Fig. 8b). Between pre- and post-drought, LDMC increased by 52.5% upstream, compared to 42.11% midstream and 35.14% downstream. The same observation holds for the relative water content (RWC, Fig. 8c). Leaves at the upstream site contained less water than those at the midstream ($p < 0.001$) and downstream sites ($p < 0.001$), however, there was no significant difference between the mid- and downstream sites ($p = 0.089$). The median RWC over the entire growing season was 70.9% at the upstream site, compared with 82.4% and 83.2% at the mid- and downstream sites, respectively. Seasonal trends in RWC (Fig. 8d) showed a decreasing trend throughout the growing season at the upstream site, with a significant difference between pre-drought and drought, and relative stabilization in the post-drought period. The pattern was similar at midstream, with a significant decrease between pre-drought and drought, followed by a non-significant increase. At the downstream site, no significant difference in RWC was observed between each drought phase. Upstream, RWC decreased by approximately -28.3% between pre-drought and post-drought, whereas it decreased by only -8.8% midstream and -6.6% downstream.

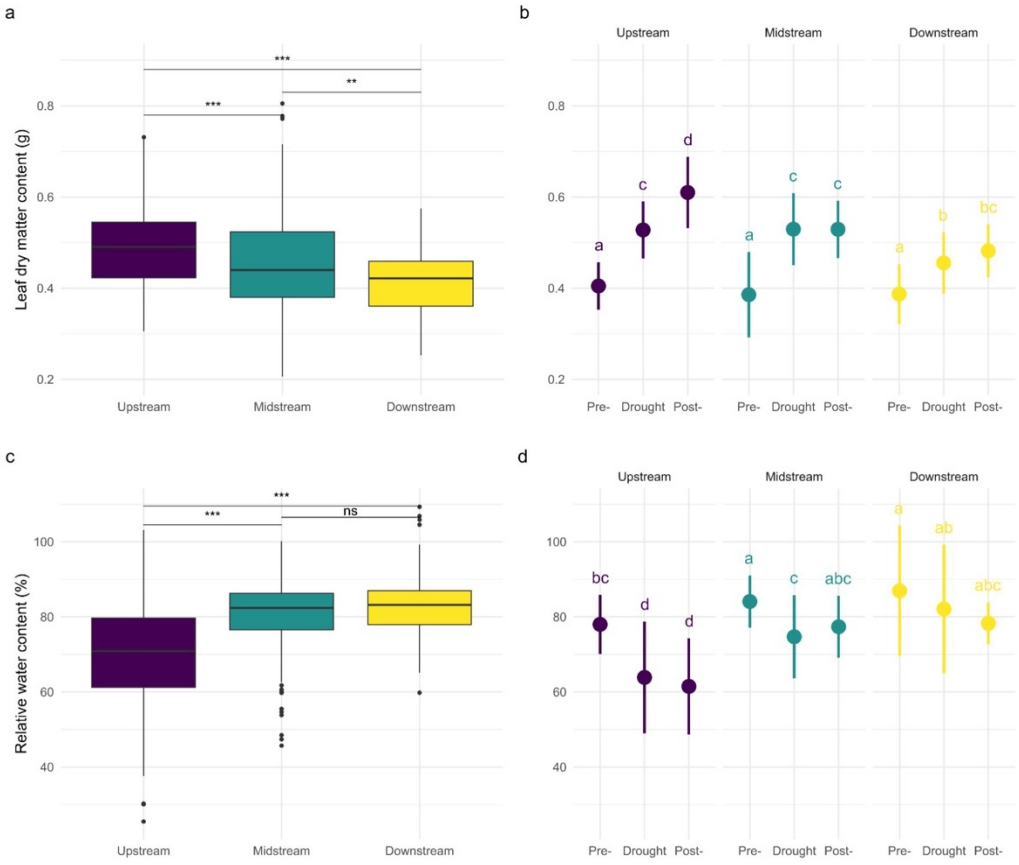

Fig. 8 - Boxplots of (a) leaf dry matter content (LDMC) and (c) relative water content (RWC) by site (upstream, midstream, downstream). Mean and standard error of (b) LDMC (d) and RWC for each drought phase and site. Colors are for site identification only. * indicates that the difference between means was statistically significant according to the Wilcoxon test. Means without common letters were significantly different at the 95% confidence level ($p < 0.05$) in Tukey's HSD post hoc tests.

3.3. Thermal imagery and ecophysiology

Analysis of canopy temperatures at the three sites showed two distinct trends (Fig. 9). First, canopy temperatures were higher than air temperatures only at midstream and downstream, while they were lower upstream. Second, only downstream showed significant differences in canopy temperatures between LWAP and HWAP plots (p = 0.002). In contrast, variability in water availability did not seem to affect canopy temperatures, as there were no significant differences in temperatures between HWAP and LWAP upstream (p = 0.63) and midstream (p = 0.48). Downstream, canopy temperatures were higher in the LWAP plot with a median of 28.56°C compared to 27.90°C in the HWAP plot. Upstream and midstream canopy temperatures in the LWAP plots had higher variability (1.05°C and 0.70°C, respectively) than those in the HWAP plots (0.23°C and 0.62°C).

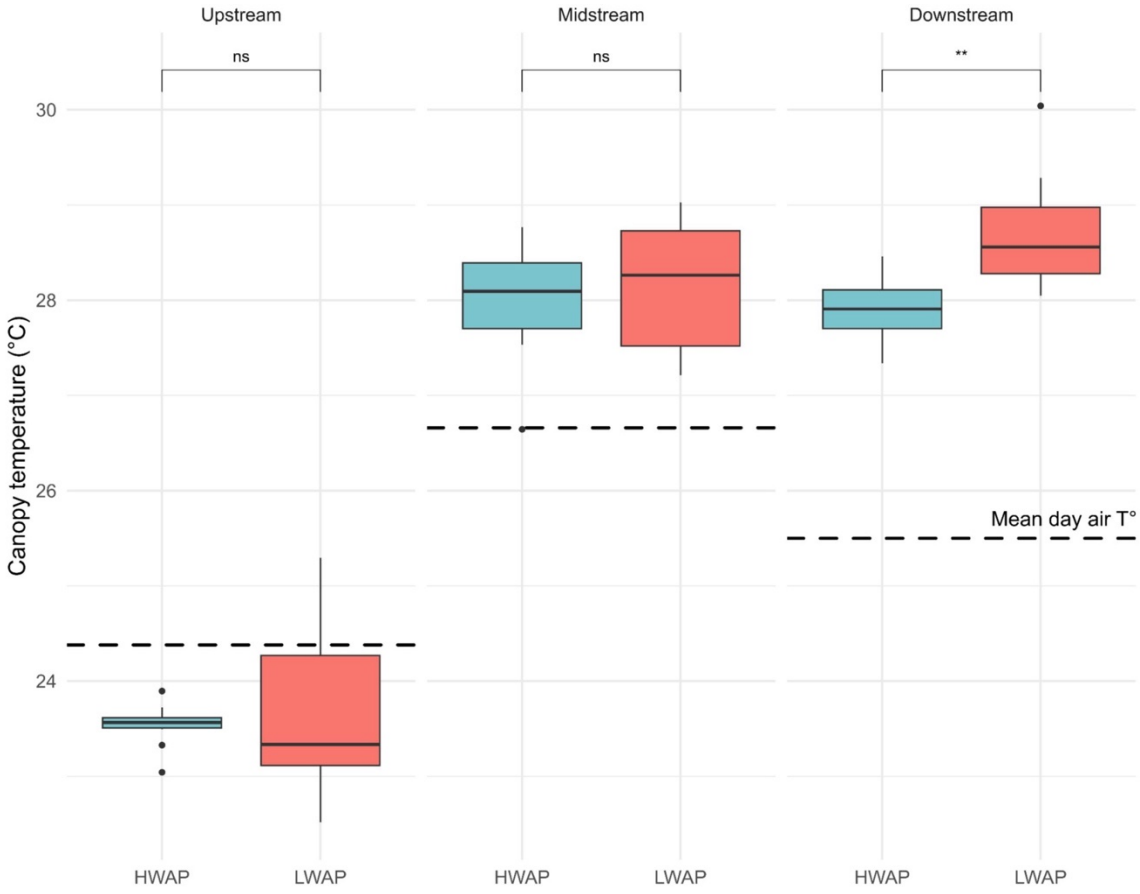

Fig. 9 - Box plots of canopy temperature for each site (upstream, midstream, downstream) and plot (HWAP and LWAP). Black dashed lines represent the mean daily air temperature at the time of the survey.

The difference between canopy temperature and air temperature (ΔT_{c-a}) showed a significant difference among the three sites (Fig. 10). Only the upstream site had a negative ΔT_{c-a}, indicating that the canopy temperature was cooler than the air temperature. In contrast, the other two sites had a positive ΔT_{c-a}, which was greater at the southernmost site. Compared to ecophysiological observations, higher relative temperature is associated with higher Ψ_m. In other words, trees with lower evapotranspiration rates had higher leaf water potentials. An opposite pattern was found for WUE_i, with lower values for mid- and downstream than for upstream.

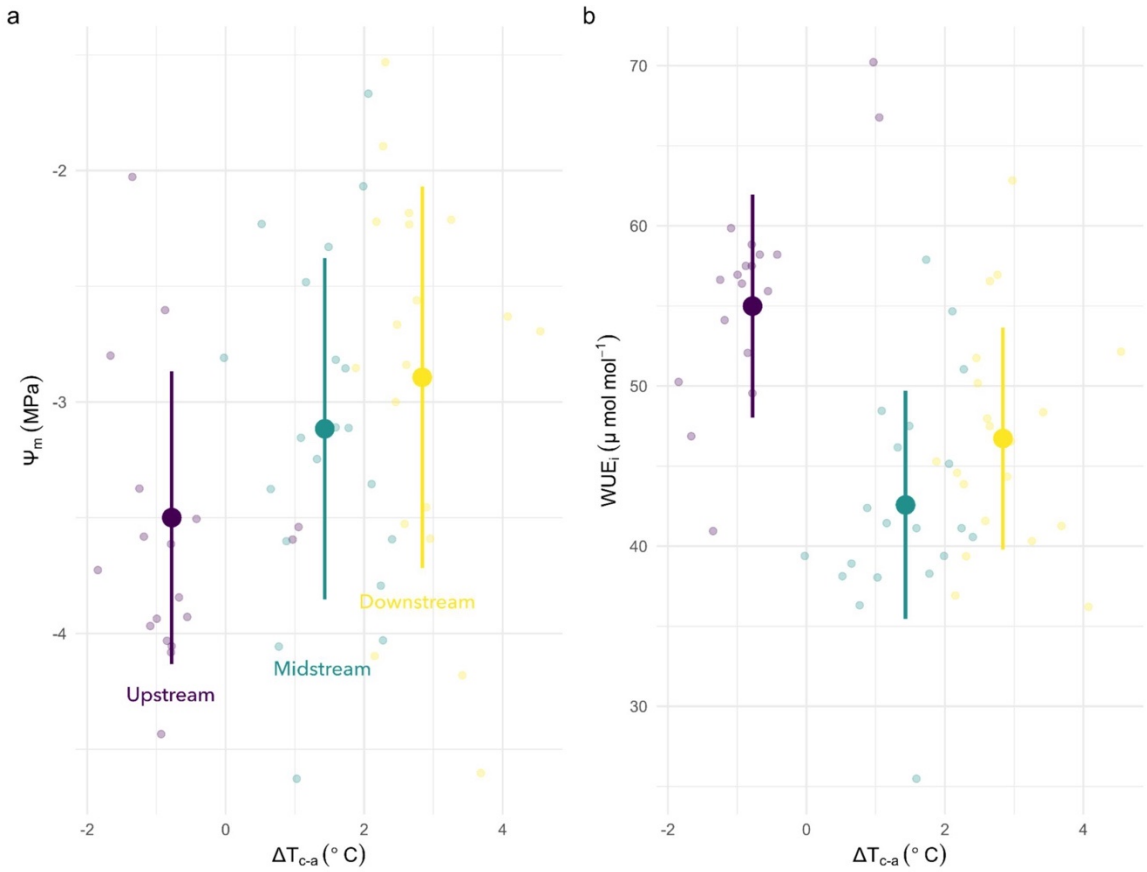

Fig. 10 - Scatterplot of (a) minimum leaf water potential and (b) water use efficiency against the difference between canopy temperature and air temperature (ΔT_{c-a}) for each site (upstream, midstream, downstream) and each plot (HWAP, LWAP). Small dots represent individual values for each tree, while large dots represent site averages. Colors are for site identification only.

3.4. Combining of airborne and satellite remote sensing approaches

Comparing remote sensing tools, a correlation can be observed between the high-resolution thermal infrared images (Fig. 11a) and the $NDVI_{Diff}$ index (Fig. 11b) hotspots at downstream. A polynomial relationship between the both rasters at each site was applied and the correlation between values was the highest at downstream (R^2 = 0.51). Midstream and downstream obtained a lower coefficient (respectively R^2 = 0.18 and R^2 =0.04).

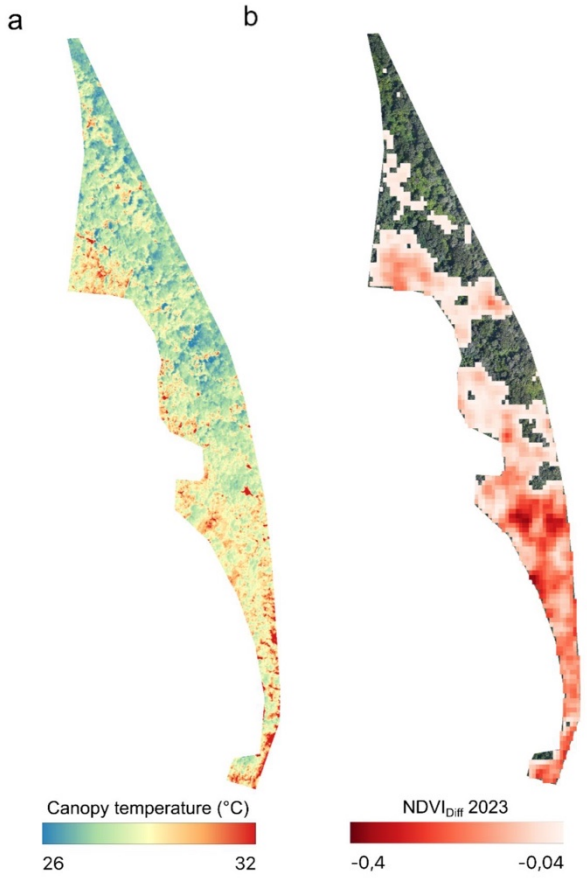

Fig. 11 (a) Canopy temperature and (b) 2023 NDVI$_{Diff}$ index over downstream site.

4. Discussion

4.1. Contrasting tree responses to seasonal drought

The upstream and downstream sites show radically different riparian tree responses to seasonal changes in drought along the hydroclimatic gradient, as shown in the conceptual model (Fig. 12). The midstream site appears to have an intermediate response, sometimes leaning more toward upstream-like and sometimes more toward downstream-like responses. This inter-site difference is also associated with intra-site variability, with contrasting responses between water stress metrics as well as between plots.

The satellite remote sensing analysis of the global canopy responses shows two distinct trends, indicating a pronounced response downstream with a decrease in NDVI during the drought, while it remains stable upstream. These responses are consistent with our field observations during the

measurements, where we observed a significant loss of leaves on trees at the downstream site during the drought, especially on the LWAP (i.e., disconnected) plot. This reduction in canopy density may partly explain the decrease in NDVI downstream. This trend in canopy density reduction was also observed in some trees at the midstream site, but not at the upstream site. These observations on the vegetative dynamics of riparian trees tend to indicate a pronounced response of tree canopy at the downstream site to drought, while those at the upstream and, to a lesser extent, midstream sites show weaker responses.

However, results obtained from the ecophysiological measurements contradict the observations made previously with remote sensing tools. In fact, leaf water potential reaches lower values upstream than at the other two sites. This observation is also valid for the relative water content, where very low values are observed upstream and decrease sharply with the seasonal evolution of the drought. In contrast, water contents are higher and more stable over the season at sites further south. The same trends can be observed with other indicators, such as leaf dry matter content, where dry matter content is higher upstream than midstream and downstream. Finally, water use efficiency also shows much greater variability upstream than downstream, indicating significant differences between tree responses. The use of thermal infrared remote sensing provides further evidence of the variability in riparian tree responses along the hydroclimatic gradient. Our results show that canopy temperatures are cooler than air temperature upstream, indicating high levels of evapotranspiration. At the same time, upstream is also the site with the lowest leaf water potential and highest WUE_i, indicating high photosynthetic activity and thus significant transpiration. This trend is completely reversed in the midstream and downstream, where canopy temperatures are warmer than air temperatures and eco-physiological indicators indicate reduced photosynthetic activity and transpiration.

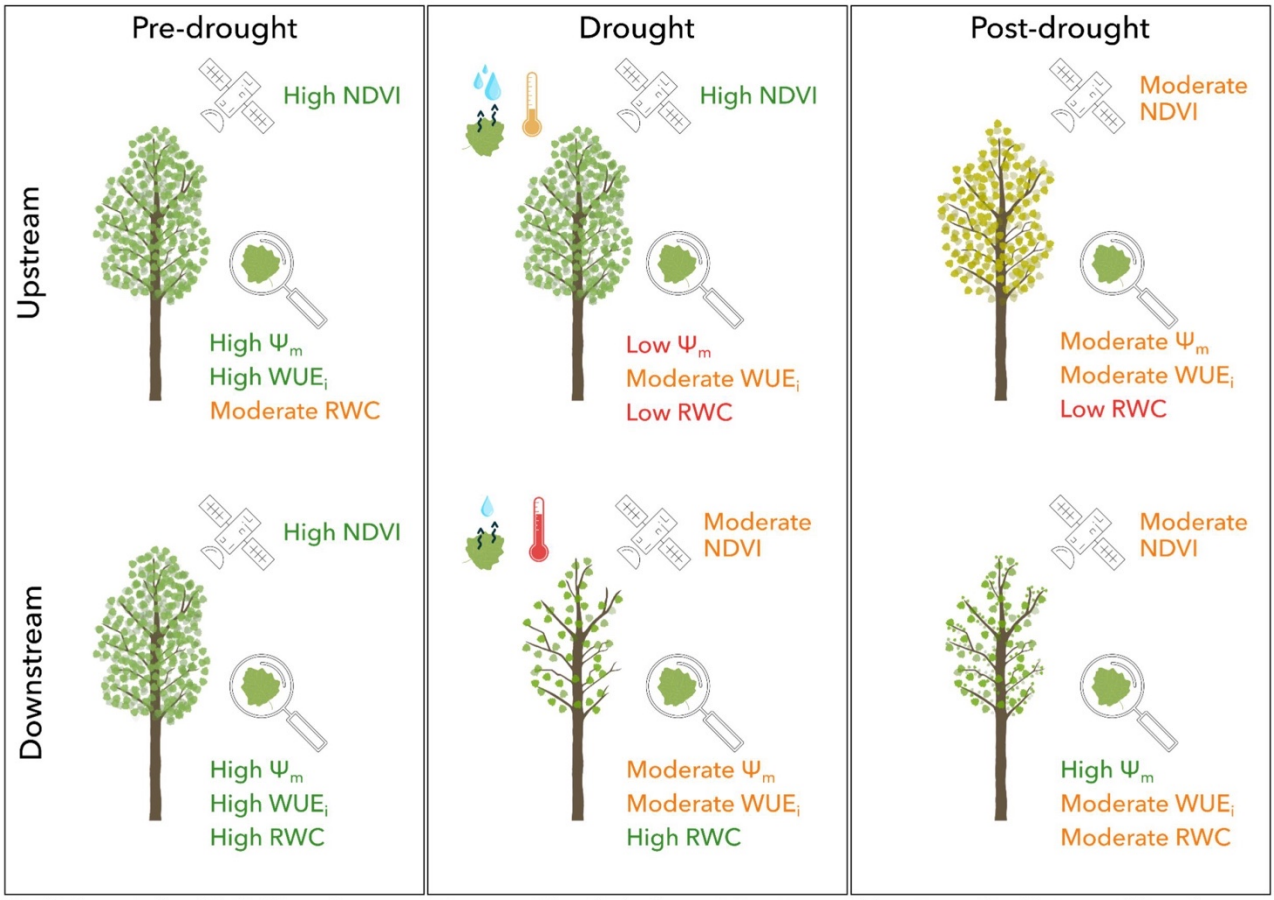

Fig. 12 Conceptual model of white poplar responses to seasonal drought development at upstream and downstream sites. Upstream white poplars adopt anisohydric behavior with high transpiration rates, resulting in low leaf water potential and water content but high NDVI. In contrast, downstream trees adopt isohydric behavior with low transpiration rates, resulting in higher leaf water potential and water content, but lower NDVI.

4.2. Contrasting behaviors and adaptations to drought and water scarcity

The different responses observed between upstream and downstream trees, as determined by both ecophysiological measurements and remote sensing, reveal nuanced adaptive behaviors within the same species in the face of drought. Downstream white poplars exhibit isohydric behavior, which allows them to rapidly limit water loss by reducing evapotranspiration through stomatal closure. With this behavior, downstream trees maintain high water potential during prolonged drought, limiting the risk of hydraulic failure. This ability highlights their better adaptation to water stress, with trees responding quickly by closing their stomata and sacrificing part of the canopy to ensure better resistance of the remaining leaves. This adaptation and resistance to water stress is probably due to their familiarity with drought coming from their location in a Mediterranean climate zone characterized by long periods of water scarcity. Upstream trees, located in a more temperate climate with few long dry periods, do not seem to benefit from this adaptive capacity. Rather than resisting stress, they try to avoid it, resulting in more diverse responses. Generally, they adopt an anisohydric behavior without reducing their evapotranspiration or limiting their water use. Their predominantly

anisohydric behavior may confer tolerance to intermittent water shortages but it also makes them vulnerable to hydraulic failure in scenarios of more intense or prolonged drought.

Increasing drought intensity and duration may affect all white poplars across the hydroclimatic gradient but at different temporal scales. Trees that are poorly adapted to drought and attempt to avoid water stress through anisohydric behavior may be rapidly exposed to hydraulic failure. On the other hand, downstream white poplars are more likely to be at risk in the long term. To identify the most vulnerable areas and the differences in behavior, it is essential to be able to combine tools and scales of measurement.

4.3. Benefits of the multi-tool approach

One of the key contribution of this work, highlighted by the contrasting responses between sites and the differing information provided by each selected tool is the importance of adopting a holistic perspective. While remote sensing provides a comprehensive view of canopy responses, ecophysiological measurements offer specific insights into the physiological mechanisms of trees. The advancement of remote sensing, whether satellite or airborne, enables the acquisition of information on forest stands at a large scale. However, these measurements need cautious interpretation, as an active vegetative state and abundant evapotranspiration do not necessarily indicate drought resistance and can imply excessive water consumption, potentially leading to irreversible turgor loss and desiccation. On the other hand, positive ecophysiological indicators, such as high water content, may illustrate stomatal closure, i.e., a slowdown in vegetative activity that can result in carbon starvation. Thus, a comprehensive understanding of forest responses to drought necessitates the integration of both remote sensing and ecophysiological metrics, acknowledging the nuances and potential trade-offs inherent in interpreting these complex ecological dynamics.

The correlation observed between our two drought indicators at downstream, despite significant disparities in scale and temporal resolution, shed light on to the dynamics of water stress in forested areas. When applied during a period of drought and over a suitable site, $NDVI_{Diff}$ index and thermal imagery can be complementing tools. TIR images having the advantage to be at higher resolution allowing to locate individuals or species with different adaptation or reactions to drought (i.e., evapotranspiration reduction) which can be used in forest management.

4.4. Limits of the method

The limited number of samples and replicates affects the robustness of the results. Moreover, the white poplar does not represent the most characteristic species of alluvial forests and has an important propensity to hybridize leading to a high genetic variability. Black poplar might have been a better candidate if it had been found at each of our study sites. Additionally, water deficit is not the sole abiotic stress affecting forest stands. A more in-depth examination of the substrate and atmospheric conditions could complement this study, providing a more holistic understanding of the multifaceted challenges faced by these forest populations.

Differences in spatial resolution and spatial extent of the remote sensing methods compared represents another limit of the method. Satellites offer high spatial coverage and temporal resolution but coarse spatial resolution. Airborne methods, while providing high spatial resolution (less than 50 $cm \cdot pixels^{-1}$), are constrained by limited spatial extent although ultralight trikes or helicopters can already cover large regions compared to drones.

The methods require specific and diverse knowledge and skills which can be a limit but which, when conducted as part of an interdisciplinary project with good coordination, turns out to be very positive.

4.5. Perspectives

With global changes leading to more intense and frequent droughts, forest managers are called upon to enhance the resilience of ecosystems. Recognizing that a given species exhibits varied responses to water stress based on its original climate, it becomes conceivable to stimulate the adaptation of a forest ecosystem to climate change by introducing young plants of species similar to the historical composition but originating from climates anticipated under future conditions. The contribution of this project points out that forest managers should not only consider the use of adapted species but also adapted traits. Individual of the same species but coming from different environment (i.e., having grown under different environmental and climatic conditions) show different behaviors in response to abiotic constraints such as water deficit. More research is needed to understand how such adaptation is passed-on to seedlings from one generation to another, which could prove significant in helping species to survive and adapt to climate change. This approach emphasizes a proactive strategy to foster ecosystem resilience, acknowledging the dynamic interplay between tree species, climate, and the evolving environmental context.

5. Conclusion

The examination of tree responses along the hydroclimatic gradient underscores the intricate interplay between environmental factors and species-specific behaviors in the face of increasing drought events. The contrasting reactions observed, particularly between upstream and downstream trees, emphasize the need for a nuanced and comprehensive approach to understand forest dynamics. The integration of remote sensing and ecophysiological measurements provides a more holistic perspective, revealing the importance of combining global insights with detailed physiological mechanisms. Furthermore, as global change intensifies drought patterns, forest managers are challenged to bolster ecosystem resilience. This approach offers a pathway to navigate the challenges posed by climate change and underscores the importance of thoughtful, anticipatory forest management practices for a sustainable and resilient future.

6. Personal contribution of the student

The student actively engaged in a collaborative research program with a team of scientists. Her involvement began with conducting a comprehensive literature review, culminating in the completion of this master's thesis. Utilizing online data such as satellite data and geomorphological data, the student identified study sites within three Nature Reserves. She took part in the selection of trees for monitoring, considering multiple constraints (see the site selection criteria detailed in the Material & Methods). She took part in sampling campaigns spanning from March to October and was subsequently involved in laboratory sample processing. She processed visible and thermal airborne images using Agisoft Metashape. The delineation of tree crowns was achieved through the analysis of processed maps and IGN high-resolution LiDAR data, enabling the extraction of the thermal signatures of individual trees. Furthermore, the student performed statistical analyses of the gathered data using R, collaborating with other scientists. Finally, beyond the redaction of this master thesis, the student contributed to the writing of a scientific paper which is about to be submitted to the international journal Global Change Biology. This collaborative effort underscored the student's comprehensive involvement in the research process and the valuable contributions she made to the project.

7. References

Aguilar, C., Zinnert, J.C., Polo, M.J., Young, D.R., 2012. NDVI as an indicator for changes in water availability to woody vegetation. Ecological Indicators 23, 290–300. https://doi.org/10.1016/j.ecolind.2012.04.008

Allen, C.D., Breshears, D.D., McDowell, N.G., 2015. On underestimation of global vulnerability to tree mortality and forest die-off from hotter drought in the Anthropocene. Ecosphere 6, 1–55. https://doi.org/10.1890/ES15-00203.1

Allen, C.D., Macalady, A.K., Chenchouni, H., Bachelet, D., McDowell, N., Vennetier, M., Kitzberger, T., Rigling, A., Breshears, D.D., Hogg, E.H. (Ted), Gonzalez, P., Fensham, R., Zhang, Z., Castro, J., Demidova, N., Lim, J.-H., Allard, G., Running, S.W., Semerci, A., Cobb, N., 2010. A global overview of drought and heat-induced tree mortality reveals emerging climate change risks for forests. Forest Ecology and Management 259, 660–684. https://doi.org/10.1016/j.foreco.2009.09.001

Allen, R.G., Food and Agriculture Organization of the United Nations (Eds.), 1998. Crop evapotranspiration: guidelines for computing crop water requirements, FAO irrigation and drainage paper. Food and Agriculture Organization of the United Nations, Rome.

Anderegg, W.R.L., Kane, J.M., Anderegg, L.D.L., 2013. Consequences of widespread tree mortality triggered by drought and temperature stress. Nature Clim Change 3, 30–36. https://doi.org/10.1038/nclimate1635

Asner, G.P., 1998. Biophysical and Biochemical Sources of Variability in Canopy Reflectance. Remote Sensing of Environment 64, 234–253. https://doi.org/10.1016/S0034-4257(98)00014-5

Beguería, S., Vicente-Serrano, S.M., Angulo-Martínez, M., 2010. A Multiscalar Global Drought Dataset: The SPEIbase: A New Gridded Product for the Analysis of Drought Variability and Impacts. Bull. Amer. Meteor. Soc. 91, 1351–1356. https://doi.org/10.1175/2010BAMS2988.1

Ben-Gal, A., Agam, N., Alchanatis, V., Cohen, Y., Yermiyahu, U., Zipori, I., Presnov, E., Sprintsin, M., Dag, A., 2009. Evaluating water stress in irrigated olives: correlation of soil water status, tree water status, and thermal imagery. Irrig Sci 27, 367–376. https://doi.org/10.1007/s00271-009-0150-7

Berg, A., Sheffield, J., 2018. Climate Change and Drought: the Soil Moisture Perspective. Curr Clim Change Rep 4, 180–191. https://doi.org/10.1007/s40641-018-0095-0

Berni, J.A.J., Zarco-Tejada, P.J., Sepulcre-Cantó, G., Fereres, E., Villalobos, F., 2009. Mapping canopy conductance and CWSI in olive orchards using high resolution thermal remote sensing imagery. Remote Sensing of Environment 113, 2380–2388. https://doi.org/10.1016/j.rse.2009.06.018

Bravard, J.-P., Gaydou, P., 2015. Historical Development and Integrated Management of the Rhône River Floodplain, from the Alps to the Camargue Delta, France, in: Hudson, P.F., Middelkoop, H. (Eds.), Geomorphic Approaches to Integrated Floodplain Management of Lowland Fluvial Systems in North America and Europe. Springer New York, New York, NY, pp. 289–320. https://doi.org/10.1007/978-1-4939-2380-9_12

Bréda, N., Huc, R., Granier, A., Dreyer, E., 2006. Temperate forest trees and stands under severe drought: a review of ecophysiological responses, adaptation processes and long-term consequences. Ann. For. Sci. 63, 625–644. https://doi.org/10.1051/forest:2006042

Choat, B., Brodribb, T.J., Brodersen, C.R., Duursma, R.A., López, R., Medlyn, B.E., 2018. Triggers of tree mortality under drought. Nature 558, 531–539. https://doi.org/10.1038/s41586-018-0240-x

Choat, B., Jansen, S., Brodribb, T.J., Cochard, H., Delzon, S., Bhaskar, R., Bucci, S.J., Feild, T.S., Gleason, S.M., Hacke, U.G., Jacobsen, A.L., Lens, F., Maherali, H., Martínez-Vilalta, J., Mayr, S., Mencuccini, M., Mitchell, P.J., Nardini, A., Pittermann, J., Pratt, R.B., Sperry, J.S., Westoby, M., Wright, I.J., Zanne, A.E., 2012. Global convergence in the vulnerability of forests to drought. Nature 491, 752–755. https://doi.org/10.1038/nature11688

Cornes, R.C., Van Der Schrier, G., Van Den Besselaar, E.J.M., Jones, P.D., 2018. An Ensemble Version of the E-OBS Temperature and Precipitation Data Sets. JGR Atmospheres 123, 9391–9409. https://doi.org/10.1029/2017JD028200

De Girolamo, A.M., Barca, E., Leone, M., Lo Porto, A., 2022. Impact of long-term climate change on flow regime in a Mediterranean basin. Journal of Hydrology: Regional Studies 41, 101061. https://doi.org/10.1016/j.ejrh.2022.101061

Evans, J.R., Von Caemmerer, S., 2013. Temperature response of carbon isotope discrimination and mesophyll conductance in tobacco. Plant Cell & Environment 36, 745–756. https://doi.org/10.1111/j.1365-3040.2012.02591.x

Friedman, J.M., Eurich, A.M., Auble, G.T., Scott, M.L., Shafroth, P.B., Gibson, P.P., 2022. Response of riparian vegetation to short- and long-term hydrologic variation. Ecological Applications 32, e2689. https://doi.org/10.1002/eap.2689

Fuchs, M., 1990. Infrared measurement of canopy temperature and detection of plant water stress. Theor Appl Climatol 42, 253–261. https://doi.org/10.1007/BF00865986

Gao, B.-C., 1995. Normalized difference water index for remote sensing of vegetation liquid water from space, in: Descour, M.R., Mooney, J.M., Perry, D.L., Illing, L.R. (Eds.), . Presented at the SPIE's 1995 Symposium on OE/Aerospace Sensing and Dual Use Photonics, Orlando, FL, United States, p. 225. https://doi.org/10.1117/12.210877

Gerle, F., Malherbe, P., Boisselet, C., Lafleuriel, D., Godfroy, J., Lochin, P., Marteau, B., Piegay, H., Puijalon, S., & Vernay, A., 2023. Intrinsic water use efficiency estimate: An isotopic method. https://www.protocols.io/view/intrinsic-water-use-efficiency-estimate-an-isotopi-c4fhytj6

Gessler, A., Rennenberg, H., Keitel, C., 2004. Stable Isotope Composition of Organic Compounds Transported in the Phloem of European Beech - Evaluation of Different Methods of Phloem Sap Collection and Assessment of Gradients in Carbon Isotope Composition during Leaf-to-Stem Transport. Plant Biology 6, 721–729. https://doi.org/10.1055/s-2004-830350

Gonzalez-Dugo, V., Zarco-Tejada, P., Berni, J.A.J., Suárez, L., Goldhamer, D., Fereres, E., 2012. Almond tree canopy temperature reveals intra-crown variability that is water stress-dependent. Agricultural and Forest Meteorology 154–155, 156–165. https://doi.org/10.1016/j.agrformet.2011.11.004

Gorelick, N., Hancher, M., Dixon, M., Ilyushchenko, S., Thau, D., Moore, R., 2017. Google Earth Engine: Planetary-scale geospatial analysis for everyone. Remote Sensing of Environment 202, 18–27. https://doi.org/10.1016/j.rse.2017.06.031

Govender, M., Govender, P., Weiersbye, I., Witkowski, E., Ahmed, F., 2009. Review of commonly used remote sensing and ground-based technologies to measure plant water stress. WSA 35. https://doi.org/10.4314/wsa.v35i5.49201

Greenwood, S., Ruiz-Benito, P., Martínez-Vilalta, J., Lloret, F., Kitzberger, T., Allen, C.D., Fensham, R., Laughlin, D.C., Kattge, J., Bönisch, G., Kraft, N.J.B., Jump, A.S., 2017. Tree mortality across biomes is promoted by drought intensity, lower wood density and higher specific leaf area. Ecology Letters 20, 539–553. https://doi.org/10.1111/ele.12748

Guinaldo, T., Voldoire, A., Waldman, R., Saux Picart, S., Roquet, H., 2023. Response of the sea surface temperature to heatwaves during the France 2022 meteorological summer. Ocean Sci. 19, 629–647. https://doi.org/10.5194/os-19-629-2023

Hartmann, H., Moura, C.F., Anderegg, W.R.L., Ruehr, N.K., Salmon, Y., Allen, C.D., Arndt, S.K., Breshears, D.D., Davi, H., Galbraith, D., Ruthrof, K.X., Wunder, J., Adams, H.D., Bloemen, J., Cailleret, M., Cobb, R., Gessler, A., Grams, T.E.E., Jansen, S., Kautz, M., Lloret, F., O'Brien, M., 2018. Research frontiers for improving our understanding of drought-induced tree and forest mortality. New Phytologist 218, 15–28. https://doi.org/10.1111/nph.15048

Hentschel, R., Hommel, R., Poschenrieder, W., Grote, R., Holst, J., Biernath, C., Gessler, A., Priesack, E., 2016. Stomatal conductance and intrinsic water use efficiency in the drought year 2003: a case study of European beech. Trees 30, 153–174. https://doi.org/10.1007/s00468-015-1284-2

Hernández-Clemente, R., Hornero, A., Mottus, M., Penuelas, J., González-Dugo, V., Jiménez, J.C., Suárez, L., Alonso, L., Zarco-Tejada, P.J., 2019. Early Diagnosis of Vegetation Health From High-

Resolution Hyperspectral and Thermal Imagery: Lessons Learned From Empirical Relationships and Radiative Transfer Modelling. Curr Forestry Rep 5, 169–183. https://doi.org/10.1007/s40725-019-00096-1

Huntjr, E., Rock, B., 1989. Detection of changes in leaf water content using Near- and Middle-Infrared reflectances☆. Remote Sensing of Environment 30, 43–54. https://doi.org/10.1016/0034-4257(89)90046-1

Isebrands, J.G., Richardson, J., 2014. Poplars and willows: trees for society and the environment. CABI, Wallingford.

Janssen, P., Stella, J.C., Piégay, H., Räpple, B., Pont, B., Faton, J.-M., Cornelissen, J.H.C., Evette, A., 2020. Divergence of riparian forest composition and functional traits from natural succession along a degraded river with multiple stressor legacies. Science of The Total Environment 721, 137730. https://doi.org/10.1016/j.scitotenv.2020.137730

Jia, Y., Zhang, B., Ma, B., 2018. Daily SPEI Reveals Long-term Change in Drought Characteristics in Southwest China. Chin. Geogr. Sci. 28, 680–693. https://doi.org/10.1007/s11769-018-0973-3

Jones, H.G., Serraj, R., Loveys, B.R., Xiong, L., Wheaton, A., Price, A.H., 2009. Thermal infrared imaging of crop canopies for the remote diagnosis and quantification of plant responses to water stress in the field. Functional Plant Biol. 36, 978. https://doi.org/10.1071/FP09123

Katul, G.G., Oren, R., Manzoni, S., Higgins, C., Parlange, M.B., 2012. Evapotranspiration: A process driving mass transport and energy exchange in the soil-plant-atmosphere-climate system. Reviews of Geophysics 50, 2011RG000366. https://doi.org/10.1029/2011RG000366

Kibler, C.L., Schmidt, E.C., Roberts, D.A., Stella, J.C., Kui, L., Lambert, A.M., Singer, M.B., 2021. A brown wave of riparian woodland mortality following groundwater declines during the 2012–2019 California drought. Environ. Res. Lett. 16, 084030. https://doi.org/10.1088/1748-9326/ac1377

Lamouroux, N., Gore, J.A., Lepori, F., Statzner, B., 2015. The ecological restoration of large rivers needs science-based, predictive tools meeting public expectations: an overview of the R hône project. Freshwater Biology 60, 1069–1084. https://doi.org/10.1111/fwb.12553

Lapidot, O., Ignat, T., Rud, R., Rog, I., Alchanatis, V., Klein, T., 2019. Use of thermal imaging to detect evaporative cooling in coniferous and broadleaved tree species of the Mediterranean maquis. Agricultural and Forest Meteorology 271, 285–294. https://doi.org/10.1016/j.agrformet.2019.02.014

Lochin, P., Piégay, H., Stella, J. C., Kelly, C., Vaudor, L., & Singer, M. B., 2023. Drivers of spatiotemporal patterns of riparian forest NDVI along a hydroclimatic gradient. In Prep.

Le, T.S., Harper, R., Dell, B., 2023. Application of Remote Sensing in Detecting and Monitoring Water Stress in Forests. Remote Sensing 15, 3360. https://doi.org/10.3390/rs15133360

Li, J., Roy, D., 2017. A Global Analysis of Sentinel-2A, Sentinel-2B and Landsat-8 Data Revisit Intervals and Implications for Terrestrial Monitoring. Remote Sensing 9, 902. https://doi.org/10.3390/rs9090902

Ma, B., Zhang, B., Jia, L., Huang, H., 2020. Conditional distribution selection for SPEI-daily and its revealed meteorological drought characteristics in China from 1961 to 2017. Atmospheric Research 246, 105108. https://doi.org/10.1016/j.atmosres.2020.105108

Ma, Q., Li, Y., Liu, F., Feng, H., Biswas, A., Zhang, Q., 2023. SPEI and multi-threshold run theory based drought analysis using multi-source products in China. Journal of Hydrology 616, 128737. https://doi.org/10.1016/j.jhydrol.2022.128737

Martinez-Vilalta, J., Anderegg, W.R.L., Sapes, G., Sala, A., 2019. Greater focus on water pools may improve our ability to understand and anticipate drought-induced mortality in plants. New Phytologist 223, 22–32. https://doi.org/10.1111/nph.15644

Marusig, D., Petruzzellis, F., Tomasella, M., Napolitano, R., Altobelli, A., Nardini, A., 2020. Correlation of Field-Measured and Remotely Sensed Plant Water Status as a Tool to Monitor the Risk of Drought-Induced Forest Decline. Forests 11, 77. https://doi.org/10.3390/f11010077

McDowell, N., Pockman, W.T., Allen, C.D., Breshears, D.D., Cobb, N., Kolb, T., Plaut, J., Sperry, J., West, A., Williams, D.G., Yepez, E.A., 2008. Mechanisms of plant survival and mortality during drought: why do some plants survive while others succumb to drought? New Phytologist 178, 719–739. https://doi.org/10.1111/j.1469-8137.2008.02436.x

McDowell, N.G., 2011. Mechanisms Linking Drought, Hydraulics, Carbon Metabolism, and Vegetation Mortality. Plant Physiology 155, 1051–1059. https://doi.org/10.1104/pp.110.170704

Medlyn, B.E., Dreyer, E., Ellsworth, D., Forstreuter, M., Harley, P.C., Kirschbaum, M.U.F., Le Roux, X., Montpied, P., Strassemeyer, J., Walcroft, A., Wang, K., Loustau, D., 2002. Temperature response of parameters of a biochemically based model of photosynthesis. II. A review of experimental data. Plant Cell & Environment 25, 1167–1179. https://doi.org/10.1046/j.1365-3040.2002.00891.x

Moatar, F., Descy, J.-P., Rodrigues, S., Souchon, Y., Floury, M., Grosbois, C., Minaudo, C., Leitao, M., Wantzen, K.M., Bertrand, F., 2022. The Loire River basin, in: Rivers of Europe. Elsevier, pp. 245–271. https://doi.org/10.1016/B978-0-08-102612-0.00007-9

Offermann, C., Ferrio, J.P., Holst, J., Grote, R., Siegwolf, R., Kayler, Z., Gessler, A., 2011. The long way down--are carbon and oxygen isotope signals in the tree ring uncoupled from canopy physiological processes? Tree Physiology 31, 1088–1102. https://doi.org/10.1093/treephys/tpr093

Pace, G., Gutiérrez-Cánovas, C., Henriques, R., Boeing, F., Cássio, F., Pascoal, C., 2021. Remote sensing depicts riparian vegetation responses to water stress in a humid Atlantic region. Science of The Total Environment 772, 145526. https://doi.org/10.1016/j.scitotenv.2021.145526

Palmer, M.A., Reidy Liermann, C.A., Nilsson, C., Flörke, M., Alcamo, J., Lake, P.S., Bond, N., 2008. Climate change and the world's river basins: anticipating management options. Frontiers in Ecology and the Environment 6, 81–89. https://doi.org/10.1890/060148

Pérez-Harguindeguy, N., Díaz, S., Garnier, E., Lavorel, S., Poorter, H., Jaureguiberry, P., Bret-Harte, M.S., Cornwell, W.K., Craine, J.M., Gurvich, D.E., Urcelay, C., Veneklaas, E.J., Reich, P.B., Poorter, L., Wright, I.J., Ray, P., Enrico, L., Pausas, J.G., De Vos, A.C., Buchmann, N., Funes, G., Quétier, F., Hodgson, J.G., Thompson, K., Morgan, H.D., Ter Steege, H., Sack, L., Blonder, B., Poschlod, P., Vaieretti, M.V., Conti, G., Staver, A.C., Aquino, S., Cornelissen, J.H.C., 2016. Corrigendum to: New handbook for standardised measurement of plant functional traits worldwide. Aust. J. Bot. 64, 715. https://doi.org/10.1071/BT12225_CO

Peters, J.M.R., López, R., Nolf, M., Hutley, L.B., Wardlaw, T., Cernusak, L.A., Choat, B., 2021. Living on the edge: A continental-scale assessment of forest vulnerability to drought. Global Change Biology 27, 3620–3641. https://doi.org/10.1111/gcb.15641

Pettit, N.E., Froend, R.H., 2018. How important is groundwater availability and stream perenniality to riparian and floodplain tree growth? Hydrological Processes 32, 1502–1514. https://doi.org/10.1002/hyp.11510

Pirasteh-Anosheh, H., Saed-Moucheshi, A., Pakniyat, H., Pessarakli, M., 2016. Stomatal responses to drought stress, in: Ahmad, P. (Ed.), Water Stress and Crop Plants. Wiley, pp. 24–40. https://doi.org/10.1002/9781119054450.ch3

Pohl, F., Rakovec, O., Rebmann, C., Hildebrandt, A., Boeing, F., Hermanns, F., Attinger, S., Samaniego, L., Kumar, R., 2023. Long-term daily hydrometeorological drought indices, soil moisture, and evapotranspiration for ICOS sites. Sci Data 10, 281. https://doi.org/10.1038/s41597-023-02192-1

Portela, A.P., Gonçalves, J.F., Durance, I., Vieira, C., Honrado, J., 2023. Riparian forest response to extreme drought is influenced by climatic context and canopy structure. Science of The Total Environment 881, 163128. https://doi.org/10.1016/j.scitotenv.2023.163128

Portier, J., Shackleton, R.T., Klesse, S., Ferretti, M., Flury, R., Hobi, M.L., Stillhard, J., Von Arx, G., Rohner, B., Thürig, E., 2023. No evidence that coring affects tree growth or mortality in three common European temperate forest tree species. Eur J Forest Res. https://doi.org/10.1007/s10342-023-01612-6

R Core Team., 2022. R: A language and environment for statistical computing. R Foundation for Statistical Computing, Vienna, Austria. [Computer software]. https://www.R-project.org/

Räpple, B., 2018. Sedimentation patterns and riparian vegetation characteristics in novel ecosystems on the Rhône River, France: A comparative approach to identify drivers and evaluate ecological potentials [These de doctorat, Lyon]. https://www.theses.fr/2018LYSEN006

Reichstein, M., Bahn, M., Ciais, P., Frank, D., Mahecha, M.D., Seneviratne, S.I., Zscheischler, J., Beer, C., Buchmann, N., Frank, D.C., Papale, D., Rammig, A., Smith, P., Thonicke, K., Van Der Velde, M., Vicca, S., Walz, A., Wattenbach, M., 2013. Climate extremes and the carbon cycle. Nature 500, 287–295. https://doi.org/10.1038/nature12350

Reichstein, M., Tenhunen, J.D., Roupsard, O., Ourcival, J., Rambal, S., Miglietta, F., Peressotti, A., Pecchiari, M., Tirone, G., Valentini, R., 2002. Severe drought effects on ecosystem CO 2 and H 2 O fluxes at three Mediterranean evergreen sites: revision of current hypotheses? Global Change Biology 8, 999–1017. https://doi.org/10.1046/j.1365-2486.2002.00530.x

Rivaes, R., Rodríguez-González, P.M., Albuquerque, A., Pinheiro, A.N., Egger, G., Ferreira, M.T., 2013. Riparian vegetation responses to altered flow regimes driven by climate change in Mediterranean rivers. Ecohydrology 6, 413–424. https://doi.org/10.1002/eco.1287

Rohde, M.M., Stella, J.C., Roberts, D.A., Singer, M.B., 2021. Groundwater dependence of riparian woodlands and the disrupting effect of anthropogenically altered streamflow. Proc. Natl. Acad. Sci. U.S.A. 118, e2026453118. https://doi.org/10.1073/pnas.2026453118

Rood, S.B., Braatne, J.H., Hughes, F.M.R., 2003. Ecophysiology of riparian cottonwoods: stream flow dependency, water relations and restoration. Tree Physiology 23, 1113–1124. https://doi.org/10.1093/treephys/23.16.1113

S. Lisar, S.Y., Motafakkerazad, R., M., M., M. Rahm, I.M., 2012. Water Stress in Plants: Causes, Effects and Responses, in: Rahman, I.Md.M. (Ed.), Water Stress. InTech. https://doi.org/10.5772/39363

Samaniego, L., Thober, S., Kumar, R., Wanders, N., Rakovec, O., Pan, M., Zink, M., Sheffield, J., Wood, E.F., Marx, A., 2018. Anthropogenic warming exacerbates European soil moisture droughts. Nature Clim Change 8, 421–426. https://doi.org/10.1038/s41558-018-0138-5

Sánchez-Pérez, J.M., Lucot, E., Bariac, T., Trémolières, M., 2008. Water uptake by trees in a riparian hardwood forest (Rhine floodplain, France). Hydrological Processes 22, 366–375. https://doi.org/10.1002/hyp.6604

Sargeant, C.I., Singer, M.B., 2021. Local and non-local controls on seasonal variations in water availability and use by riparian trees along a hydroclimatic gradient. Environ. Res. Lett. 16, 084018. https://doi.org/10.1088/1748-9326/ac1294

Sauquet, E., Richard, B., Devers, A., Prudhomme, C., 2019. Water restrictions under climate change: a Rhône–Mediterranean perspective combining bottom-up and top-down approaches. Hydrol. Earth Syst. Sci. 23, 3683–3710. https://doi.org/10.5194/hess-23-3683-2019

Scholander, P.F., Bradstreet, E.D., Hemmingsen, E.A., Hammel, H.T., 1965. Sap Pressure in Vascular Plants: Negative hydrostatic pressure can be measured in plants. Science 148, 339–346. https://doi.org/10.1126/science.148.3668.339

Seibt, U., Rajabi, A., Griffiths, H., Berry, J.A., 2008. Carbon isotopes and water use efficiency: sense and sensitivity. Oecologia 155, 441–454. https://doi.org/10.1007/s00442-007-0932-7

Sevanto, S., Mcdowell, N.G., Dickman, L.T., Pangle, R., Pockman, W.T., 2014. How do trees die? A test of the hydraulic failure and carbon starvation hypotheses. Plant Cell & Environment 37, 153–161. https://doi.org/10.1111/pce.12141

Shafroth, P.B., Stromberg, J.C., Patten, D.T., 2002. RIPARIAN VEGETATION RESPONSE TO ALTERED DISTURBANCE AND STRESS REGIMES. Ecological Applications 12, 107–123. https://doi.org/10.1890/1051-0761(2002)012[0107:RVRTAD]2.0.CO;2

Singer, M.B., Stella, J.C., Dufour, S., Piégay, H., Wilson, R.J.S., Johnstone, L., 2013. Contrasting water-uptake and growth responses to drought in co-occurring riparian tree species. Ecohydrology 6, 402–412. https://doi.org/10.1002/eco.1283

Slette, I.J., Post, A.K., Awad, M., Even, T., Punzalan, A., Williams, S., Smith, M.D., Knapp, A.K., 2019. How ecologists define drought, and why we should do better. Global Change Biology 25, 3193–3200. https://doi.org/10.1111/gcb.14747

Smart, R.E., Bingham, G.E., 1974. Rapid Estimates of Relative Water Content. Plant Physiol. 53, 258–260. https://doi.org/10.1104/pp.53.2.258

Stella, J.C., Battles, J.J., 2010. How do riparian woody seedlings survive seasonal drought? Oecologia 164, 579–590. https://doi.org/10.1007/s00442-010-1657-6

Still, C., Powell, R., Aubrecht, D., Kim, Y., Helliker, B., Roberts, D., Richardson, A.D., Goulden, M., 2019. Thermal imaging in plant and ecosystem ecology: applications and challenges. Ecosphere 10, e02768. https://doi.org/10.1002/ecs2.2768

Stromberg, J.C., Tiller, R., Richter, B., 1996. Effects of Groundwater Decline on Riparian Vegetation of Semiarid Regions: The San Pedro, Arizona. Ecological Applications 6, 113–131. https://doi.org/10.2307/2269558

Surendar, K.K., Devi, D.D., Ravi, I., Jeyakumar, P., Velayudham, K., 2013. Effect of Water Stress on Leaf Temperature, Transpiration Rate, Stomatal Diffusive Resistance and Yield of Banana. pgt. https://doi.org/10.5376/pgt.2013.04.0008

Teskey, R.O., Hinckley, T.M., 1986. Moisture: Effects of Water Stress on Trees, in: Hennessey, T.C., Dougherty, P.M., Kossuth, S.V., Johnson, J.D. (Eds.), Stress Physiology and Forest Productivity, Forestry Sciences. Springer Netherlands, Dordrecht, pp. 9–33. https://doi.org/10.1007/978-94-009-4424-4_2

Théroux-Rancourt, G., Éthier, G., Pepin, S., 2014. Threshold response of mesophyll CO 2 conductance to leaf hydraulics in highly transpiring hybrid poplar clones exposed to soil drying. EXBOTJ 65, 741–753. https://doi.org/10.1093/jxb/ert436

Tripathy, K.P., Mishra, A.K., 2023. How Unusual Is the 2022 European Compound Drought and Heatwave Event? Geophysical Research Letters 50, e2023GL105453. https://doi.org/10.1029/2023GL105453

Tucker, C.J., 1980. Remote sensing of leaf water content in the near infrared. Remote Sensing of Environment 10, 23–32. https://doi.org/10.1016/0034-4257(80)90096-6

Vernay, A., Tian, X., Chi, J., Linder, S., Mäkelä, A., Oren, R., Peichl, M., Stangl, Z.R., Tor-Ngern, P., Marshall, J.D., 2020. Estimating canopy gross primary production by combining phloem stable isotopes with canopy and mesophyll conductances. Plant Cell & Environment 43, 2124–2142. https://doi.org/10.1111/pce.13835

Vicente-Serrano, S.M., Beguería, S., López-Moreno, J.I., 2010. A Multiscalar Drought Index Sensitive to Global Warming: The Standardized Precipitation Evapotranspiration Index. Journal of Climate 23, 1696–1718. https://doi.org/10.1175/2009JCLI2909.1

Wang, Q., Wu, J., Lei, T., He, B., Wu, Z., Liu, M., Mo, X., Geng, G., Li, X., Zhou, H., Liu, D., 2014. Temporal-spatial characteristics of severe drought events and their impact on agriculture on a global scale. Quaternary International 349, 10–21. https://doi.org/10.1016/j.quaint.2014.06.021

Wang, Q., Zeng, J., Qi, J., Zhang, X., Zeng, Y., Shui, W., Xu, Z., Zhang, R., Wu, X., Cong, J., 2021. A multi-scale daily SPEI dataset for drought characterization at observation stations over mainland China from 1961 to 2018. Earth Syst. Sci. Data 13, 331–341. https://doi.org/10.5194/essd-13-331-2021

Williams, J., Stella, J.C., Voelker, S.L., Lambert, A.M., Pelletier, L.M., Drake, J.E., Friedman, J.M., Roberts, D.A., Singer, M.B., 2022. Local groundwater decline exacerbates response of dryland riparian woodlands to climatic drought. Global Change Biology 28, 6771–6788. https://doi.org/10.1111/gcb.16376

Yakir, D., Sternberg, L.D.S.L., 2000. The use of stable isotopes to study ecosystem gas exchange. Oecologia 123, 297–311. https://doi.org/10.1007/s004420051016

Zarco-Tejada, P.J., Rueda, C.A., Ustin, S.L., 2003. Water content estimation in vegetation with MODIS reflectance data and model inversion methods. Remote Sensing of Environment 85, 109–124. https://doi.org/10.1016/S0034-4257(02)00197-9

Zhang, R., Bento, V.A., Qi, J., Xu, F., Wu, J., Qiu, J., Li, J., Shui, W., Wang, Q., 2023. The first high spatial resolution multi-scale daily SPI and SPEI raster dataset for drought monitoring and

evaluating over China from 1979 to 2018. Big Earth Data 7, 860–885.
https://doi.org/10.1080/20964471.2022.2148331

8. Supplementary information

8.1. Data summary

	Sampling date	Measure	Number of samplings	mean	sd
Upstream	2023-04-20	WUE	19	47.188	8.872
	2023-05-15	WUE	20	47.797	9.030
	2023-05-15	Ψm	40	-1.524	0.319
	2023-06-05	WUE	19	50.822	8.162
	2023-06-05	Ψm	38	-1.936	0.828
	2023-06-26	WUE	19	45.508	9.746
	2023-06-26	Ψm	40	-3.246	0.732
	2023-07-17	WUE	19	54.459	7.094
	2023-07-17	Ψm	40	-3.499	0.705
	2023-07-17	Thermal	18	23.611	0.688
	2023-08-21	Ψm	40	-3.394	1.229
	2023-09-06	WUE	19	38.093	8.596
	2023-09-06	Ψm	38	-3.403	0.831
	2023-10-04	Ψm	36	-2.919	0.571
Midstream	2023-04-27	WUE	19	46.501	6.847
	2023-04-27	Ψm	39	-1.803	0.327
	2023-05-16	WUE	20	49.464	6.908
	2023-05-16	Ψm	40	-1.473	0.373
	2023-06-06	WUE	20	50.010	7.212
	2023-06-06	Ψm	40	-2.048	0.263
	2023-06-29	WUE	20	49.910	8.398
	2023-06-29	Ψm	40	-3.570	0.984
	2023-07-18	WUE	20	42.480	7.124
	2023-07-18	Ψm	40	-3.116	0.739
	2023-07-18	Thermal	20	28.099	0.644
	2023-08-18	Ψm	40	-2.795	0.629
	2023-09-07	WUE	18	39.329	7.629
	2023-09-07	Ψm	34	-3.422	0.402
	2023-10-04	Ψm	36	-3.090	0.762
Downstream	2023-04-24	WUE	19	44.826	8.452
	2023-04-24	Ψm	40	-1.497	0.374
	2023-05-15	WUE	20	49.868	7.446
	2023-05-15	Ψm	40	-1.953	0.354
	2023-06-05	WUE	19	51.067	8.296
	2023-06-05	Ψm	38	-2.160	0.600
	2023-06-27	Ψm	38	-2.652	0.548
	2023-07-12	WUE	19	47.070	6.887
	2023-07-12	Ψm	38	-2.893	0.884
	2023-07-12	Thermal	20	28.305	0.630
	2023-07-12	ndvi	20	0.588	0.038
	2023-08-17	Ψm	38	-2.847	0.664
	2023-09-07	WUE	16	44.571	8.330
	2023-09-07	Ψm	34	-3.197	0.771
	2023-10-03	Ψm	34	-2.030	0.767

8.2. Table of used packages in RStudio

Package	Version	Description
Data Manipulation		
dplyr	1.0.10	Data manipulation and transformation.
lidR	4.0.3	Airborne LiDAR interface for data maipulation and visualisation
lubridate	1.9.2	Provides tools that make it easier to parse and manipulate dates.
purrr	1.0.2	Simplifies working with functions and vectors.
raster	3.6-26	Geographic data analysis and modeling. Reads and writes 'tif' file formats
reshape2	1.4.4	Reshapes and transforms data.
rgl	1.2.1	Provides functions for 3D interactive graphics
rlas	1.6.3	Reads and writes 'las' and 'laz' binary file formats
sf	1.0-14	Handles spatial data using simple features.
sjmisc	2.8.9	Contains functions for data cleaning and transformation.
tidyr	1.3.0	Reshapes and tidies data.
Statistical Analysis		
broom	1.0.5	Converts statistical analysis objects into tidy data frames.
emmeans	1.9.0	Estimates marginal means and contrasts.
jtools	2.2.2	Enhances the output of statistical models, providing tools for summarizing, plotting, and interpreting model results.
lme4	1.1-34	Used for fitting linear mixed-effects models.
moments	0.14.1	Computes statistical moments, such as mean, variance, skewness, and kurtosis.
multcomp	1.4-25	Performs multiple comparisons after a significant ANOVA result.
multcompView	0.1-9	Provides tools for visualizing and interpreting multiple comparisons.
MuMIn	1.47.5	Supports model selection and model averaging.
rstatix	0.7.2	Provides a set of functions for easy statistical analysis and visualization.
sjPlot	2.8.14	Creates tables and plots for statistical models fitted with various packages, including lme4.
Visualization		
cowplot	1.1.1	Enhances ggplot2 with functions for combining multiple plots.
ggplot2	3.4.4	Creates static, animated, and interactive plots using a grammar of graphics.
ggpubr	0.6.0	Extends ggplot2 with functions for combining and annotating plots. Simplifies the creation of complex plots.
ggsignif	0.6.4	Adds easy-to-read significance markers to ggplot2 plots.
gt	0.9.0	Creates tables with a modern look.
patchwork	1.1.3	Allows for the composition of multiple ggplot2 plots into a single plot.
viridis	0.6.4	A color palette for data visualizations designed to be perceptually uniform and readable by those with color vision deficiencies.